ETH zürich

Interaction between charge, spin and orbital currents in magnetic heterostructures

P. Gambardella

Department of Materials, ETH Zürich, Switzerland

G. Sala
V. Krizakova
G. Krishnaswamy
E. Grimaldi
M. Wörnle
C.-H. Lambert
D. Phuong
S. Velez

ETH Zürich

Z. Luo
A. Hrabec
S. Finizio
S. Wintz
J. Raabe
L. Heyderman

PSI

M. Weigand

HZB Helmholtz Zentrum Berlin

S. Couet
K. Garello
F. Yasin
G.S. Kar

imec

P. Welter
C. Degen

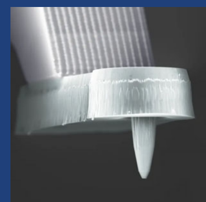

ZABRE

Outline

- Charge-spin conversion mechanisms
- Spin-orbit torques
- Current-induced manipulation of
  - ✓ Ferromagnets
  - ✓ Ferrimagnets
  - ✓ Antiferromagnets
- Examples of applications
  - ✓ Domain wall logic
  - ✓ MRAMs

Spin currents

Spin polarized current

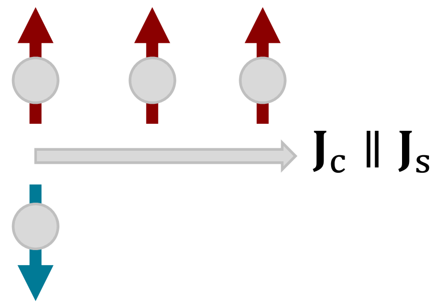

Tunnelling Magnetoresistance (TMR)

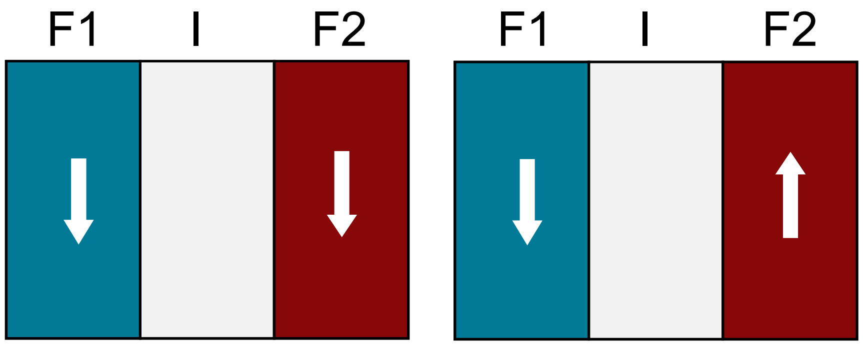

small resistance = 0 large resistance = 1

Spin torques

Spin polarized current

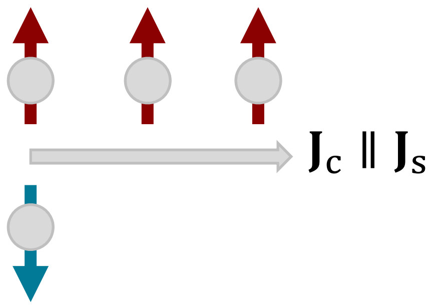

Spin transfer torque

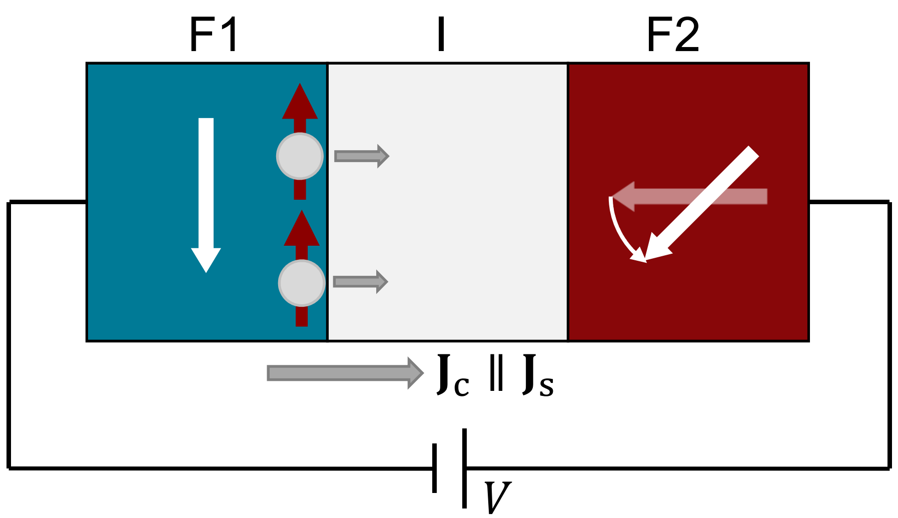

ETH zürich

Magnetic random access memories (MRAMs)

Ferrite-core memory 1955-1975

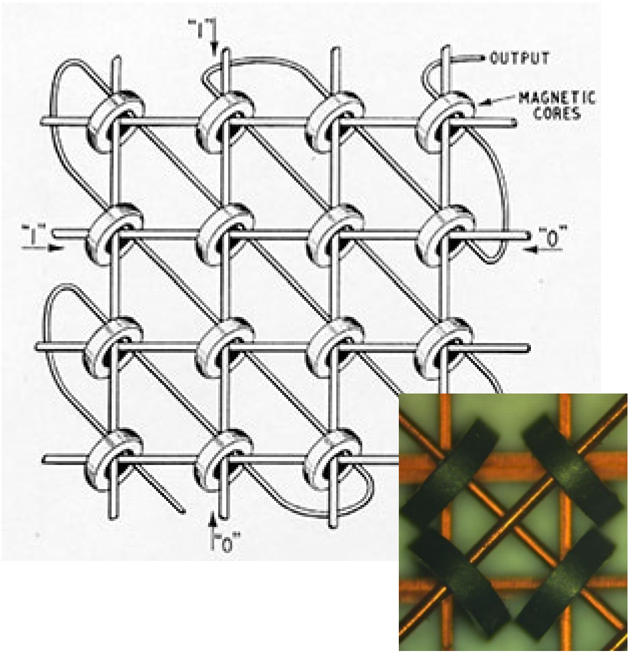

STT-MRAM

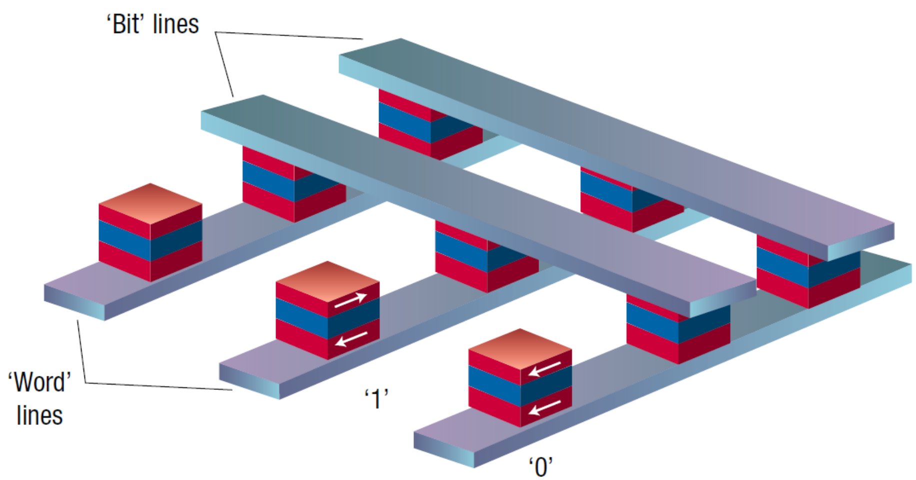

Chappert, Fert & Van Dau, Nat. Mater. 2007
Dieny et al., Nat. Electronics 2020

	Ferrite core memory	STT-MRAM
Density	32 kb/ft^3 Pitch (size) 5 mm (1 mm)	1 Gb/cm^2 Pitch (size) 100 nm (50 nm)
Writing Speed	> 1 ms	10 ns
Switching current Switching energy of 1 bit	100-500 mA 1-5 10^{-7} J	50 μA 1-5 10^{-13} J
Endurance	?	10^{12-14} cycles

Embedded memories: Present

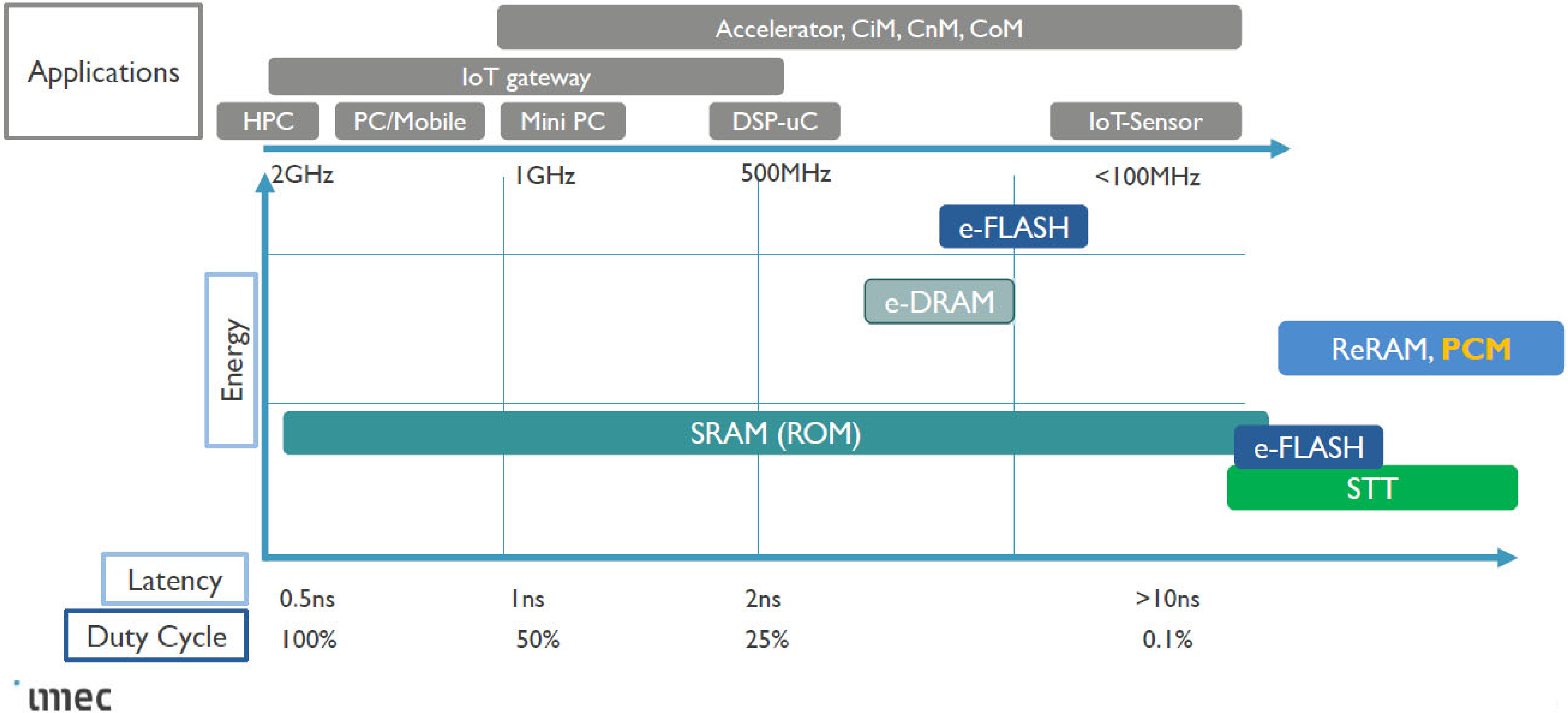

V. Krizakova *et al.*, *J. Magn. Magn. Mater.* **562**, 169692 (2022)

Electronic *vs* spin memories

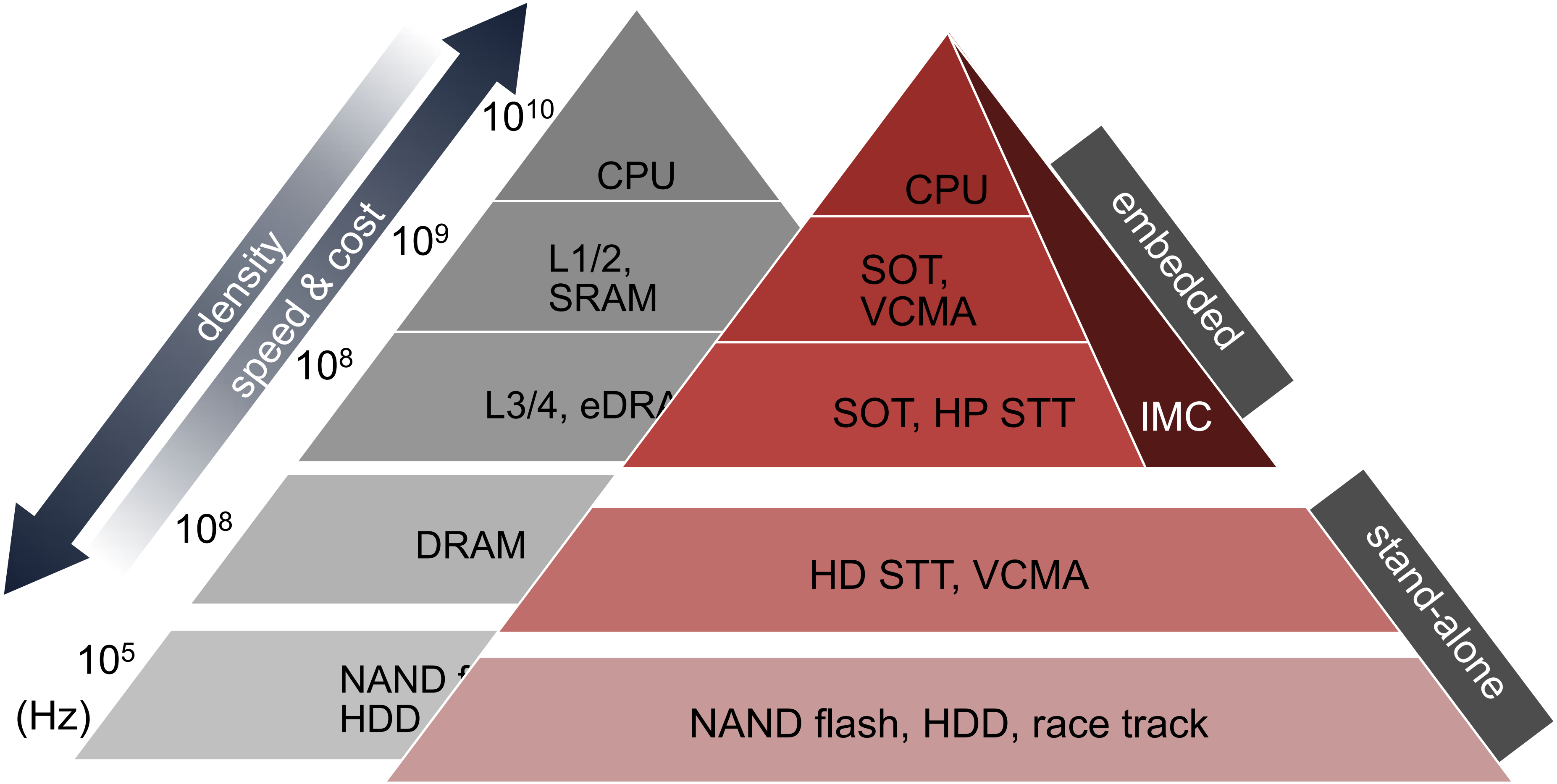

V. Krizakova *et al.*, *J. Magn. Magn. Mater.* **562**, 169692 (2022)

Charge-spin interconversion mechanisms

Charge-to-orbital conversion
Orbital Hall effect
Orbital Rashba effect

Magnetoresistance
Magnetoelectric coupling

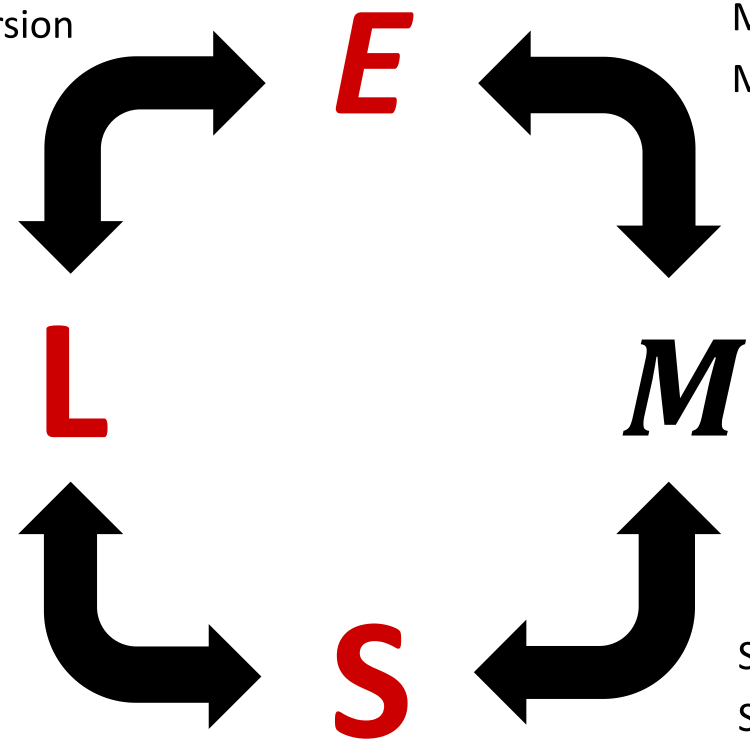

Orbital-to-spin conversion
Spin Hall effect
Rashba-Edelstein effect

Spin torques
Spin pumping

Currents of angular momentum

Pure charge current | Spin-polarized current | Pure spin current

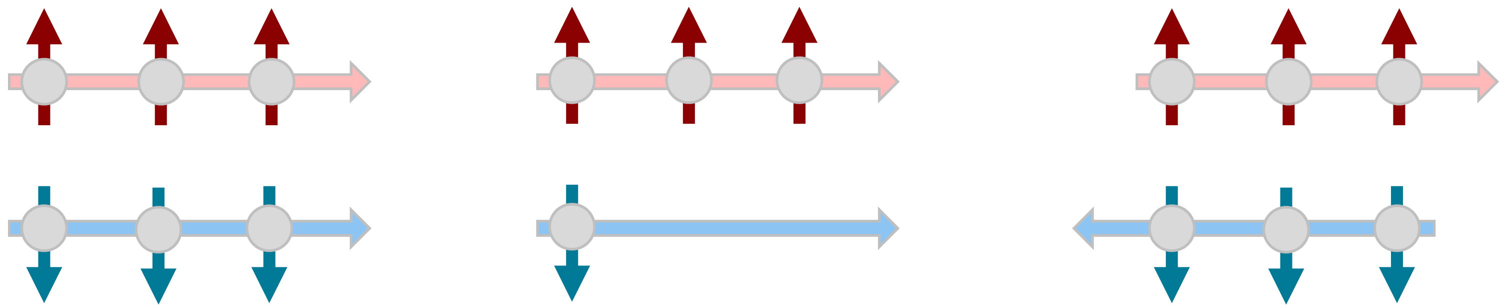

$\mathbf{J_c} \neq 0, \mathbf{J_s} = 0$ | $\mathbf{J_c} \parallel \mathbf{J_s}$ | $\mathbf{J_c} = 0, \mathbf{J_s} \neq 0$

$$\mathbf{J_c} = \mathbf{J_\uparrow} + \mathbf{J_\downarrow}$$

$$\mathbf{J_s} = -\frac{\hbar}{2e}(\mathbf{J_\uparrow} - \mathbf{J_\downarrow})$$

The spin Hall effect

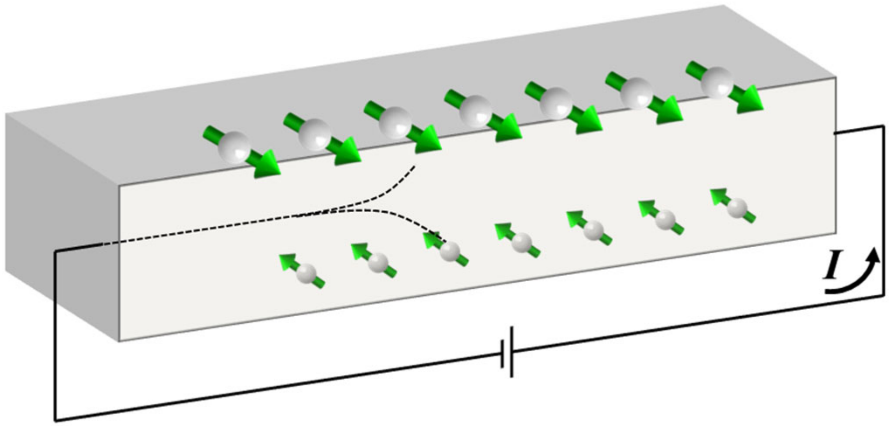

Dyakonov and Perel, JETP Lett. **13**, 467 (1971)
Sinova et al., Rev. Mod. Phys. **87**, 1213 (2015)

Spin-dependent anomalous velocity:

$$\boldsymbol{v} = \frac{1}{\hbar}\frac{\partial E_n(\boldsymbol{k})}{\partial \boldsymbol{k}} + \dot{\boldsymbol{k}} \times \boldsymbol{\Omega}_n(\boldsymbol{k})$$

Karplus and Lüttinger, Phys. Rev. **95**, 1154 (1954)
Xiao, Chang and Niu, Rev. Mod. Phys. **82**, 1959 (2010)

$$j^s_{zy} = \theta_{SH}\, j^c_x$$

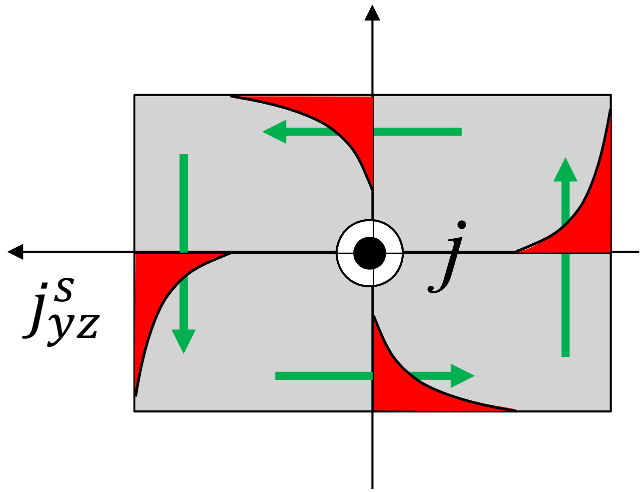

$$\theta_{SH} = \frac{j_s}{j_c} = \frac{\sigma^{SH}_{yx}}{\sigma_{xx}}$$

$$\theta_{SH}(\mathrm{Pt}) = 0.05 - 0.2$$

$$\lambda_s(\mathrm{Pt}) = 1 - 14\ nm$$

MOKE detection of the SHE-induced spin accumulation in Pt

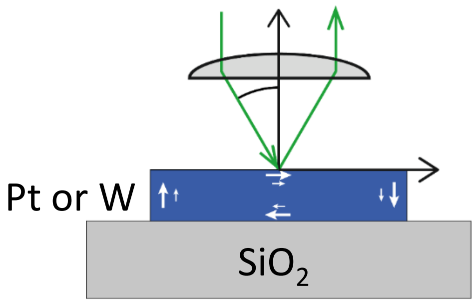

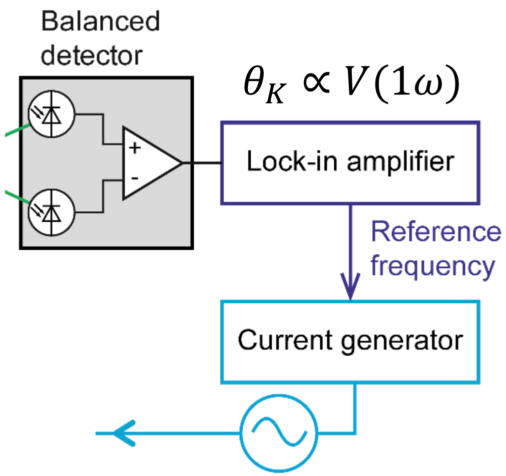

$I = I_0 \sin \omega t$

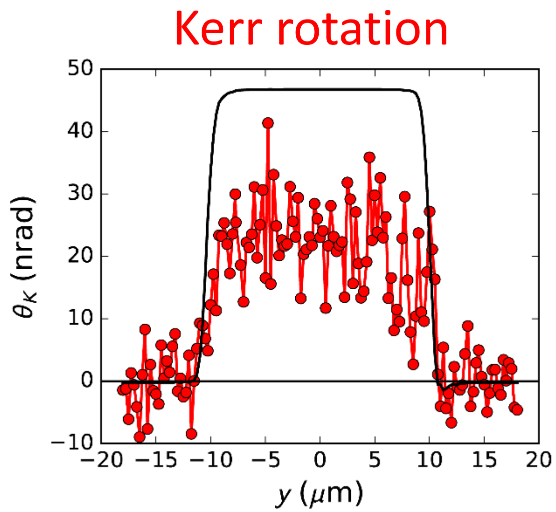

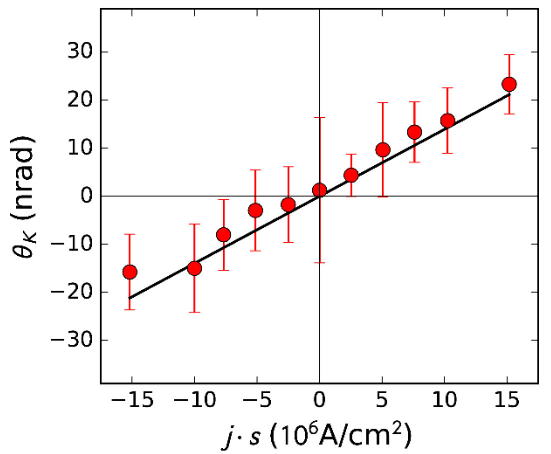

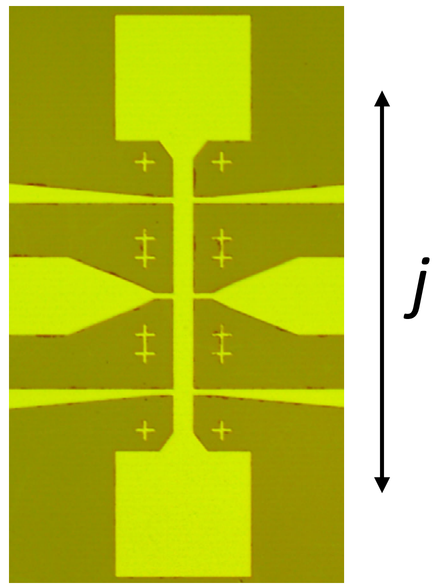

Stamm, PG et al., *PRL* **119**, 087203 (2017)

MOKE detection of SHE-induced spin accumulation

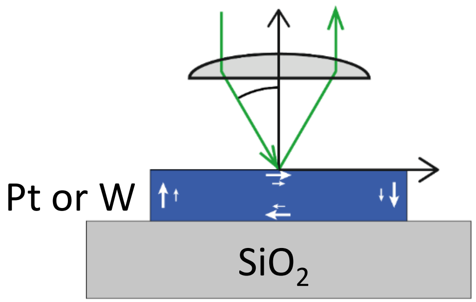

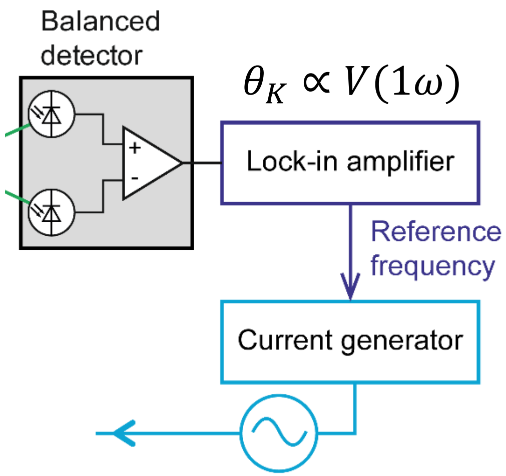

$I = I_0 \sin \omega t$

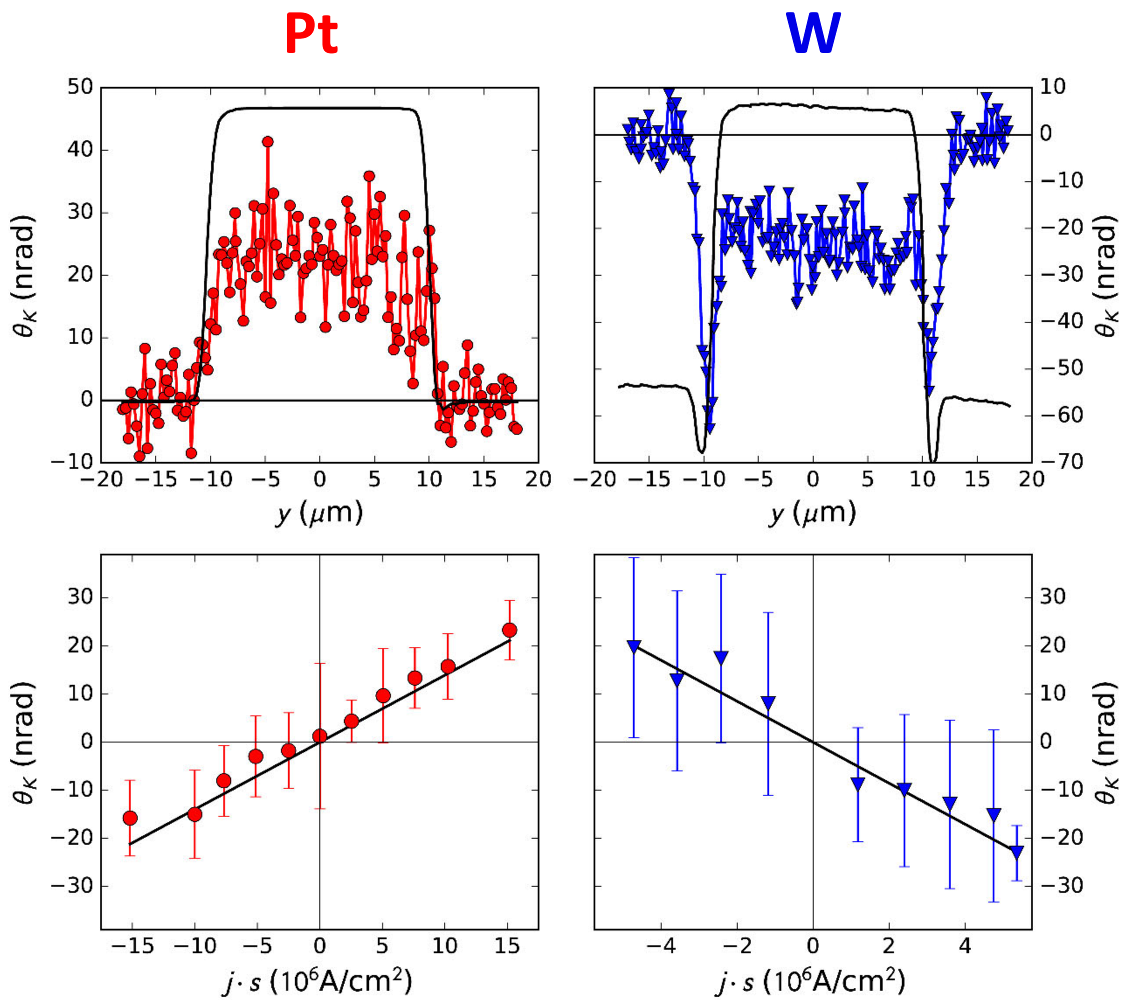

$$\frac{\theta_K}{j} = 14\,\frac{nrad}{10^7 A/cm^2}$$

$$\frac{\theta_K}{j} = -43\,\frac{nrad}{10^7 A/cm^2}$$

Stamm et al., *PRL* **119**, 087203 (2017)

Rashba-Edelstein effect

$$E_{+/-} = \frac{\hbar^2 k^2}{2m^*} +/- \alpha_R k$$

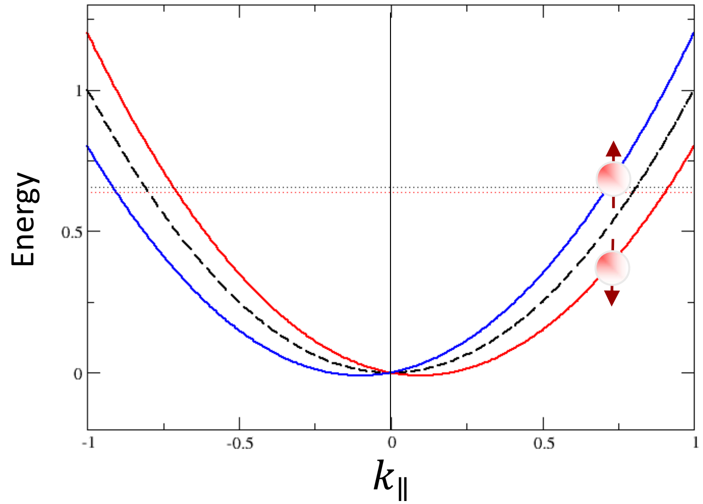

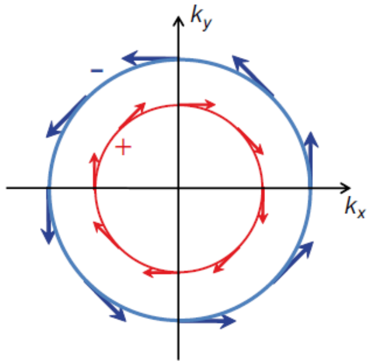

Manchon and Zhang, PRB **78**, 212405 (2008)
PG and Miron, Phil. Trans. R. Soc. A **369**, 3175 (2011)

Currents of angular momentum

Pure charge current

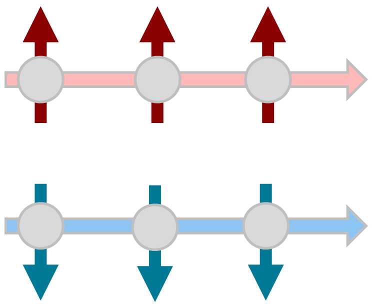

$\mathbf{J_c} \neq 0, \mathbf{J_s} = 0$

Spin-polarized current

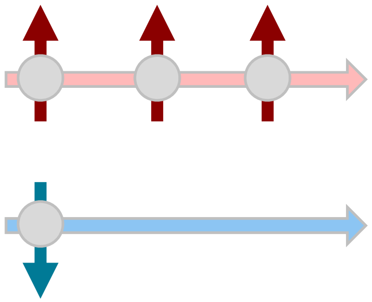

$\mathbf{J_c} \parallel \mathbf{J_s}$

Pure spin current

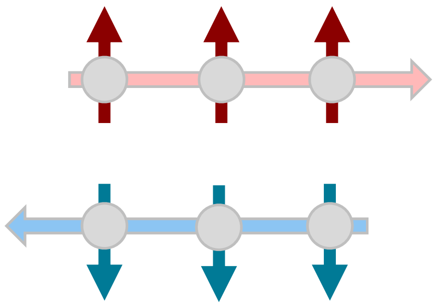

$\mathbf{J_c} = 0, \mathbf{J_s} \neq 0$

$$\mathbf{J_c} = \mathbf{J_\uparrow} + \mathbf{J_\downarrow}$$
$$\mathbf{J_S} = -\frac{\hbar}{2e}(\mathbf{J_\uparrow} - \mathbf{J_\downarrow})$$

Pure orbital current

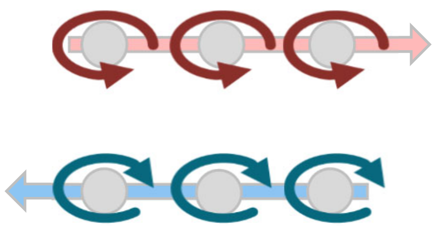

$\mathbf{J_c} = 0, \mathbf{J_L} \neq 0$

Bernevig et al., PRL 2005

Orbital Hall and spin Hall conductivities in the transition metals

$$j_L = \sigma_{yx}^{OH} E$$

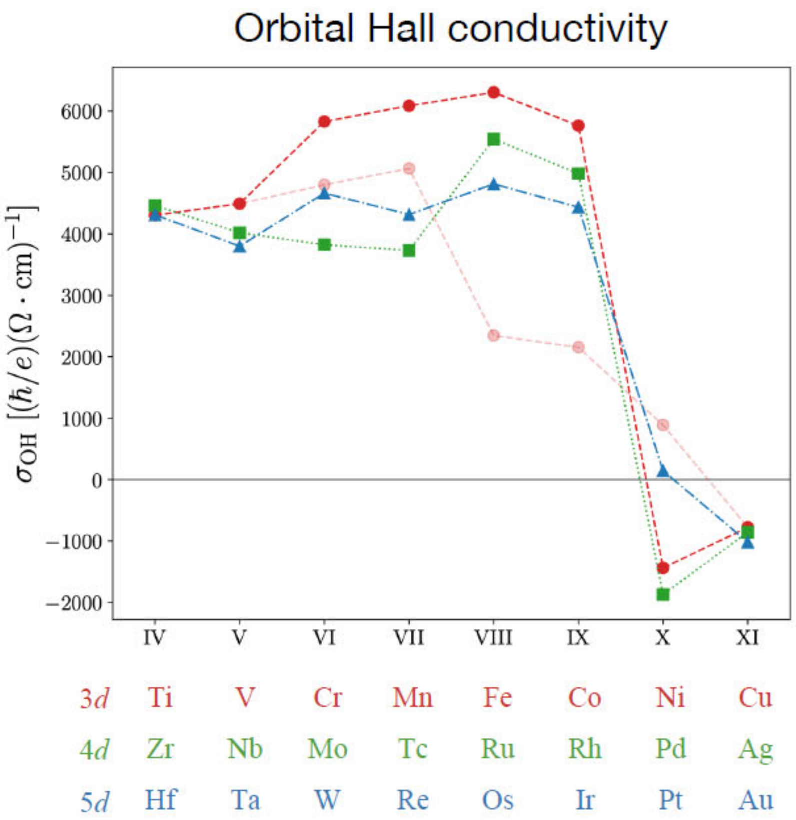

$$j_S = \sigma_{yx}^{SH} E$$

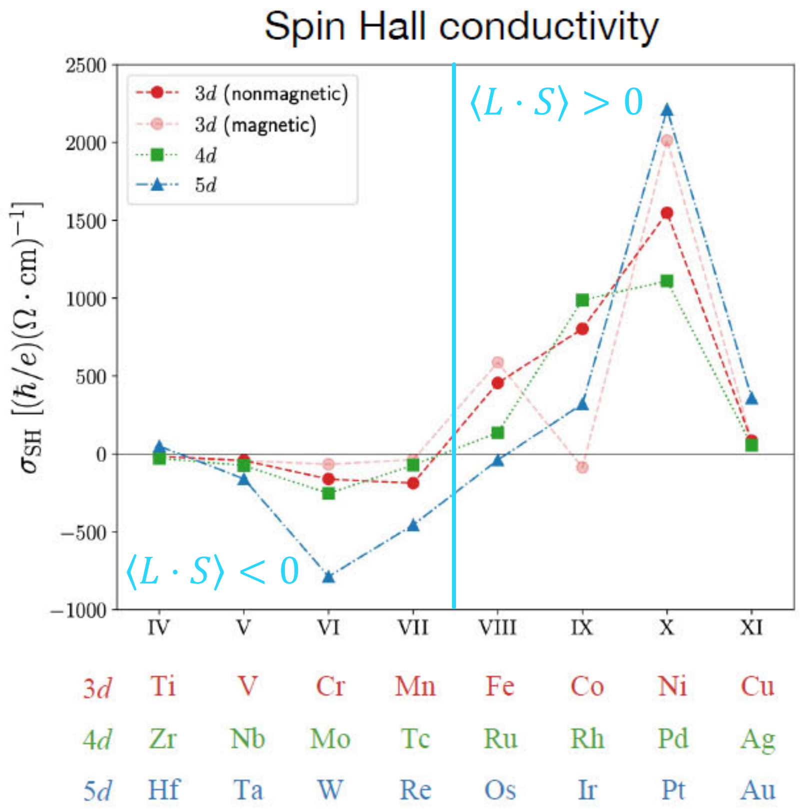

Dongwook Go & Yury Mokrousov, to be published
see also Salemi and Oppeneer, Phys. Rev. Mater. **6**, 095001 (2022)

Charge and spin conversion mechanisms

SHE

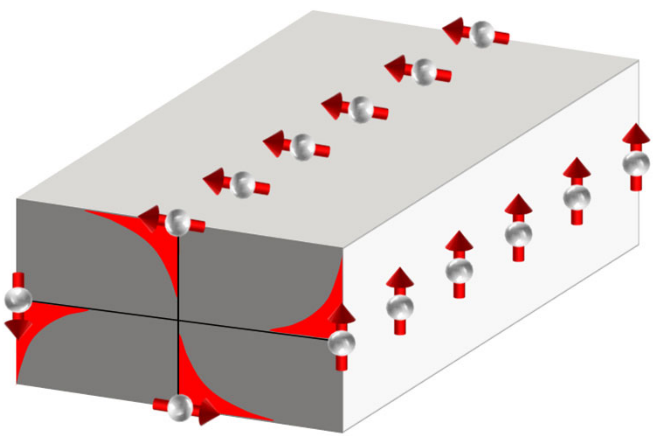

Sinova et al., Rev. Mod. Phys. **87**, 1213 (2015)

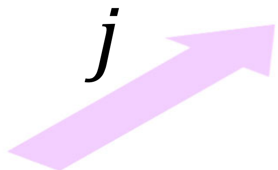

OHE

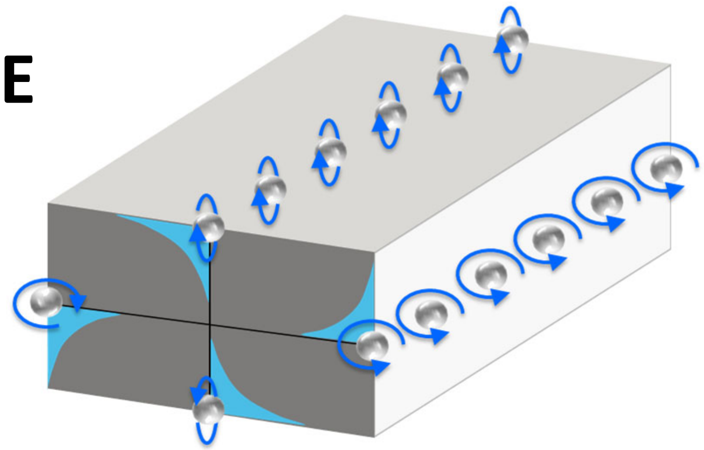

Kontani et al., PRL 1**02**, 016601 (2009)
Go et al., PRL **121**, 086602 (2018)

REE

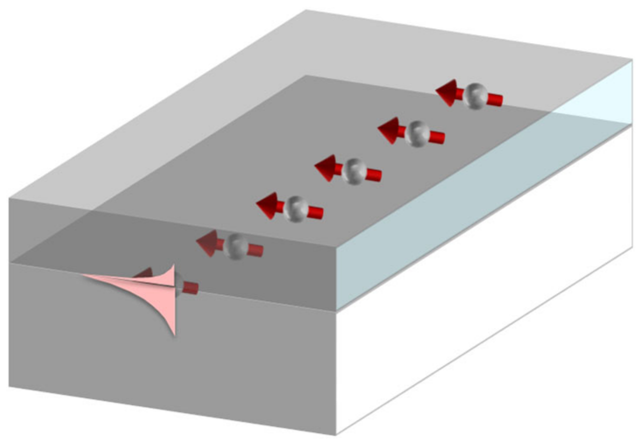

Manchon and Zhang, PRB **78**, 212405 (2008)
PG and Miron, Phil. Trans. R. Soc. A **369**, 3175 (2011)

OREE

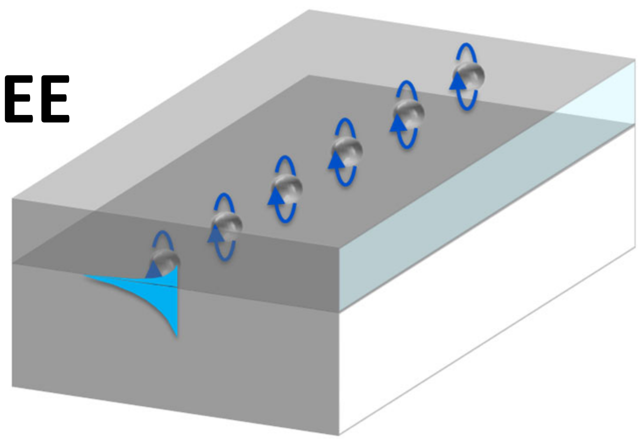

Salemi et al., , Nat. Comm. **10**, 5381 (2019)

Current-induced spin-orbit torques in FM/NM bilayers

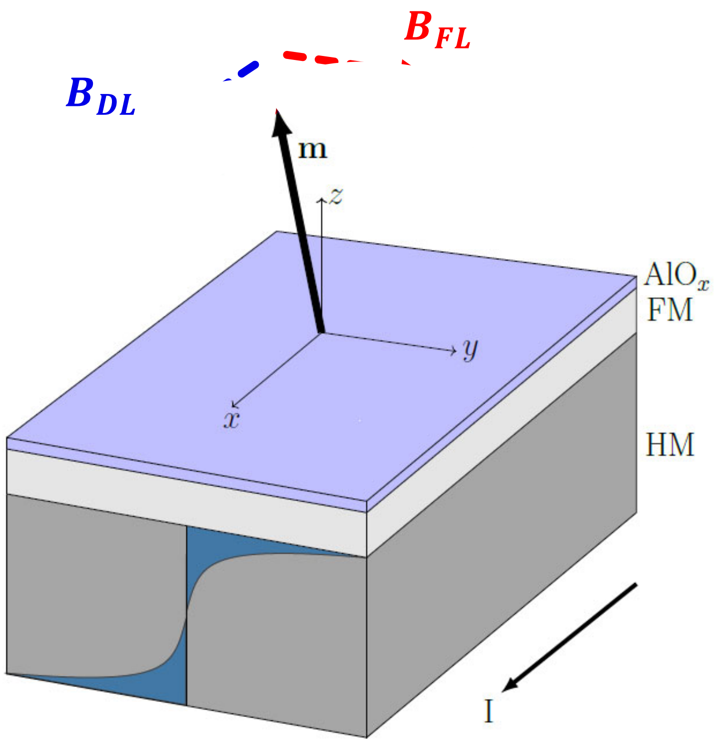

"Bulk" spin current

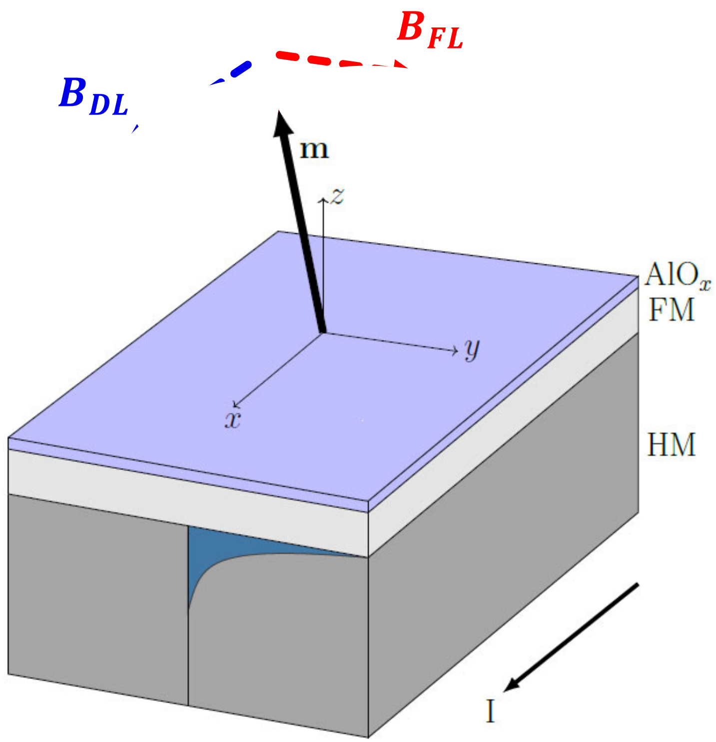

Interfacial spin polarization

Manchon et al., Rev. Mod. Phys. **91**, 035004 (2019)

Orbital torque in Co and Ni layers due to OHE in Cr and Mn

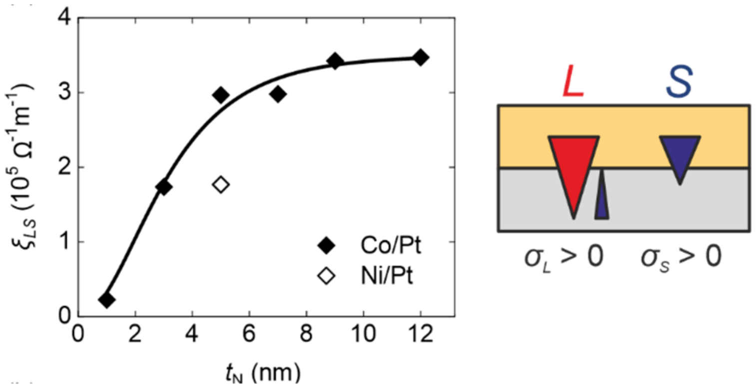

- «Standard» spin-orbit torque in Co/Pt and Ni/Pt due to spin current generated by Pt

G. Sala and PG, Phys. Rev. Res. **4**, 033037 (2022)

Orbital torque in Co and Ni layers due to OHE in Cr and Mn

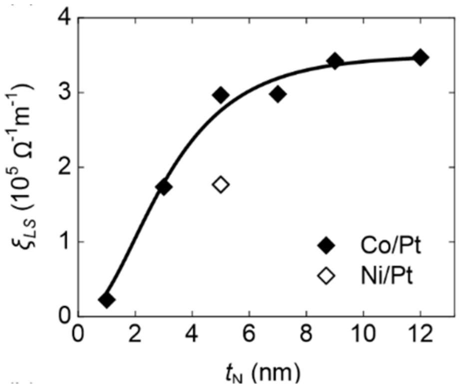

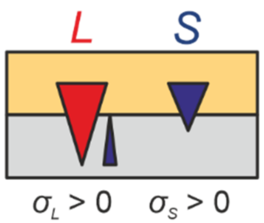

- «Standard» spin-orbit torque in Co/Pt and Ni/Pt due to spin current generated by Pt

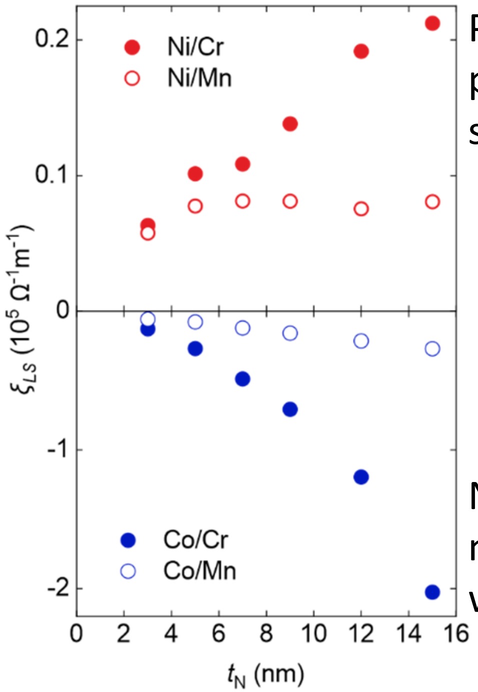

Positive torque due to positive OHE in Cr and strong $\langle L\cdot S\rangle$>0 in Ni

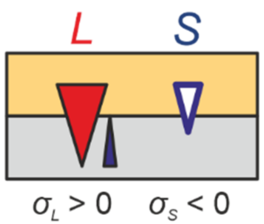

Negative torque due to negative SHE in Cr and weak $\langle L\cdot S\rangle$>0 in Co

- Orbital torque in Ni,Co/Cr due to orbital current and spin current generated by Cr

	Cr	Mn	Co	Ni
$\langle \mathbf{L}\cdot\mathbf{S}\rangle$	−	−	+	+
σ_L	+	+		+
σ_S	−	−	+	+

G. Sala and PG, Phys. Rev. Res. **4**, 033037 (2022)

Crucial role of orbital-to-spin conversion

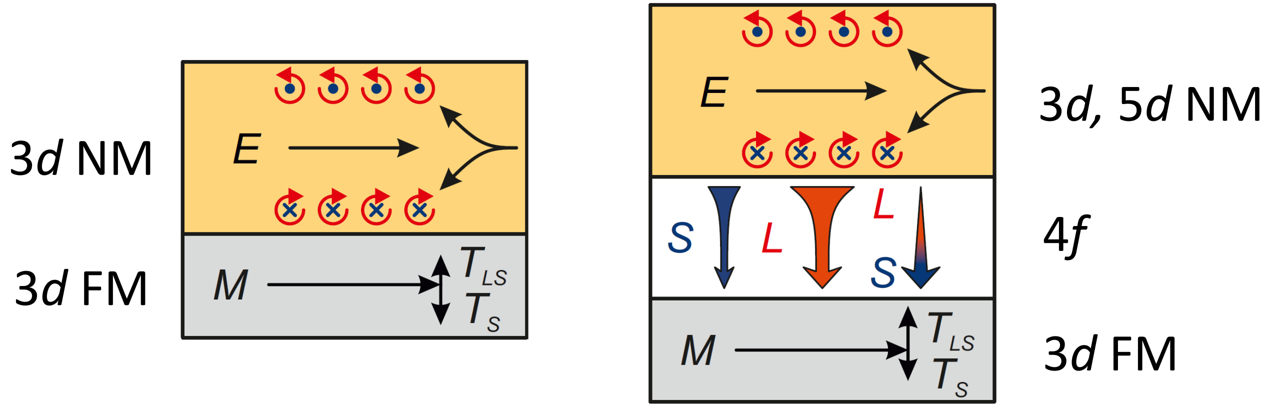

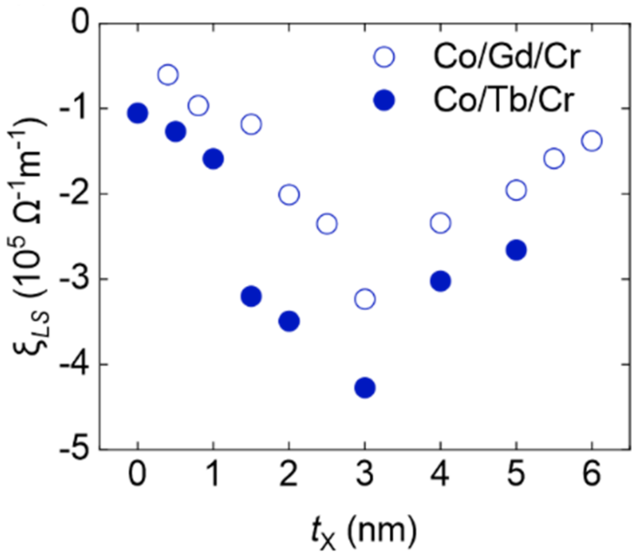

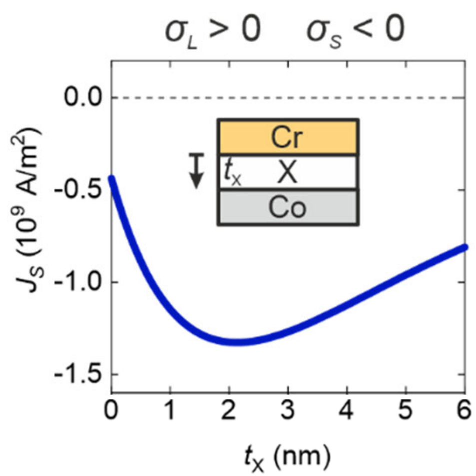

$$\frac{d^2\mu_S}{dz^2} = \frac{\mu_S}{\lambda_S^2} \pm \frac{\mu_L}{\lambda_{LS}^2}$$

$$\frac{d^2\mu_L}{dz^2} = \frac{\mu_L}{\lambda_L^2} \pm \frac{\mu_S}{\lambda_{LS}^2},$$

$$j_S = -\frac{\sigma}{2e}\frac{d\mu_S}{dz} + \sigma_S E,$$

$$j_L = -\frac{\sigma}{2e}\frac{d\mu_L}{dz} + \sigma_L E,$$

G. Sala and PG, Phys. Rev. Res. **4**, 033037 (2022)

Giant orbital Hall effect in metallic heterostructures

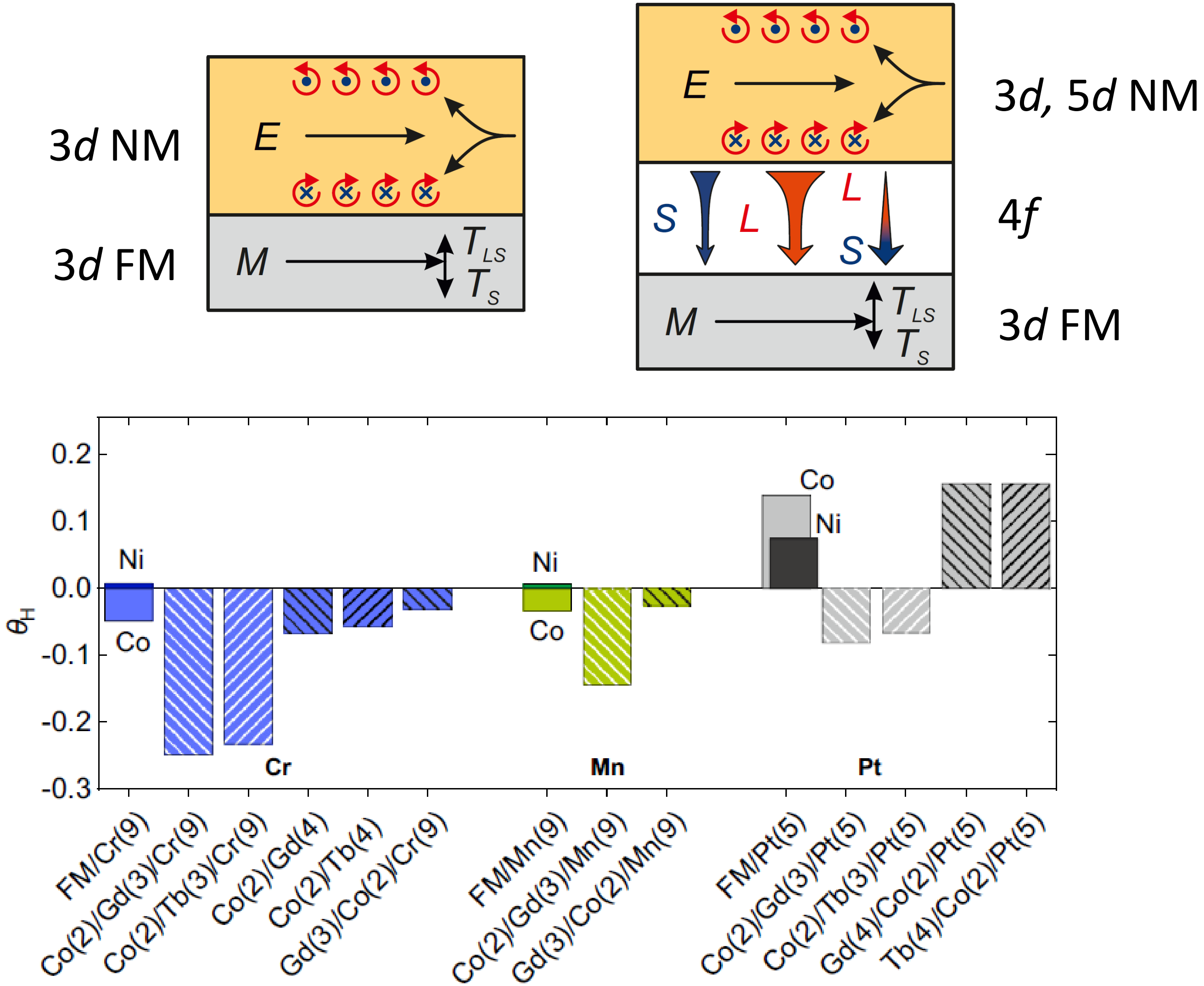

G. Sala and PG, Phys. Rev. Res. **4**, 033037 (2022)

Charge-spin conversion and spin-orbit torques

Functionalities & applications

Magnetization switching

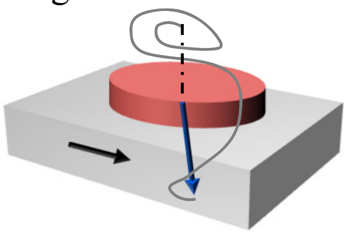

Magnetic memories

High-frequency oscillations

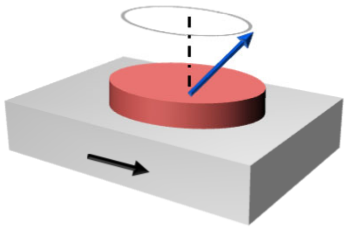

GHz and THz nanooscillators

Domain wall and skyrmion motion

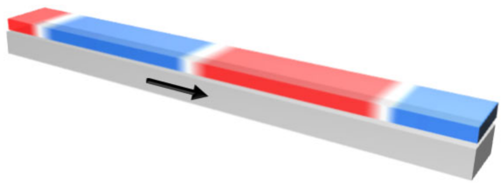

Race-track memories

Spin-wave excitations

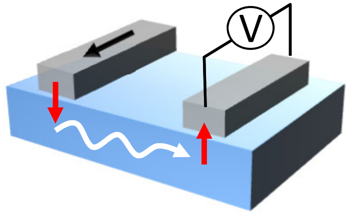

Chargeless interconnect & spin logic

Materials

Magnetic metallic heterostructures

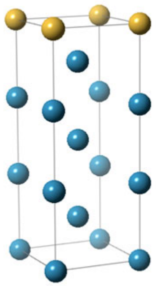

Co, Ni, Fe, GdFeCo...
Pt, W, Ta…
WO_x, CuO_x , $SrIrO_3$...
Bi_2Se_3, WTe_2, MoS_2...

Magnetic Insulators (YIG, TmIG, Bi:YIG…)

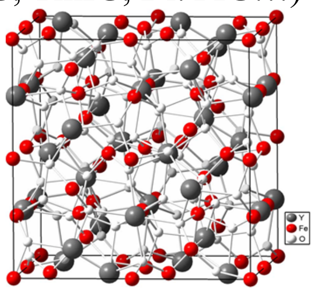

2D Materials

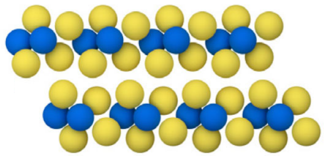

Antiferromagnets (CuMnAs, Mn_2Au, IrMn…)

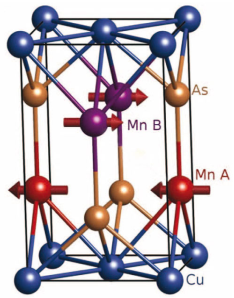

Manchon et al., Rev. Mod. Phys. **91**, 035004 (2019)

Spin-orbit torques acting on domain walls

Bloch walls

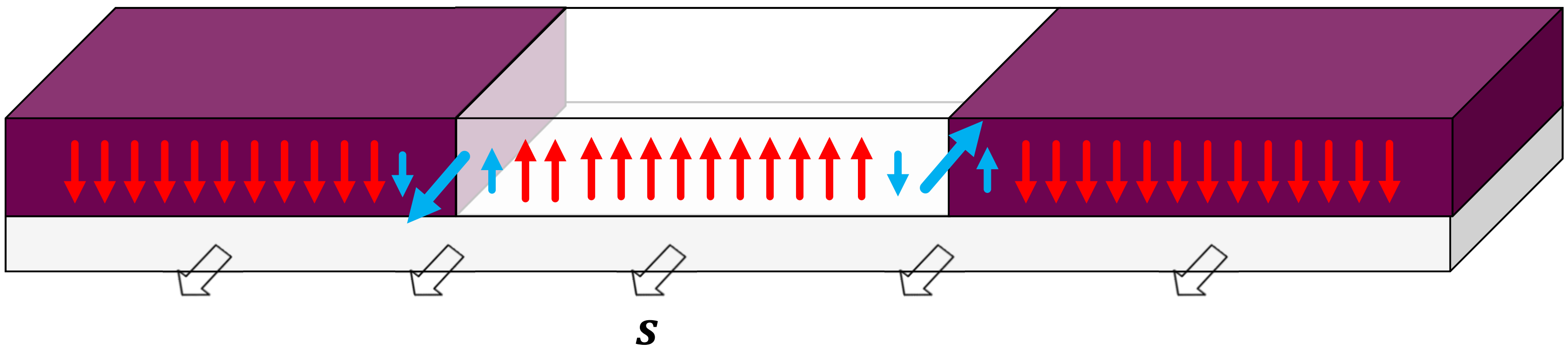

Néel walls

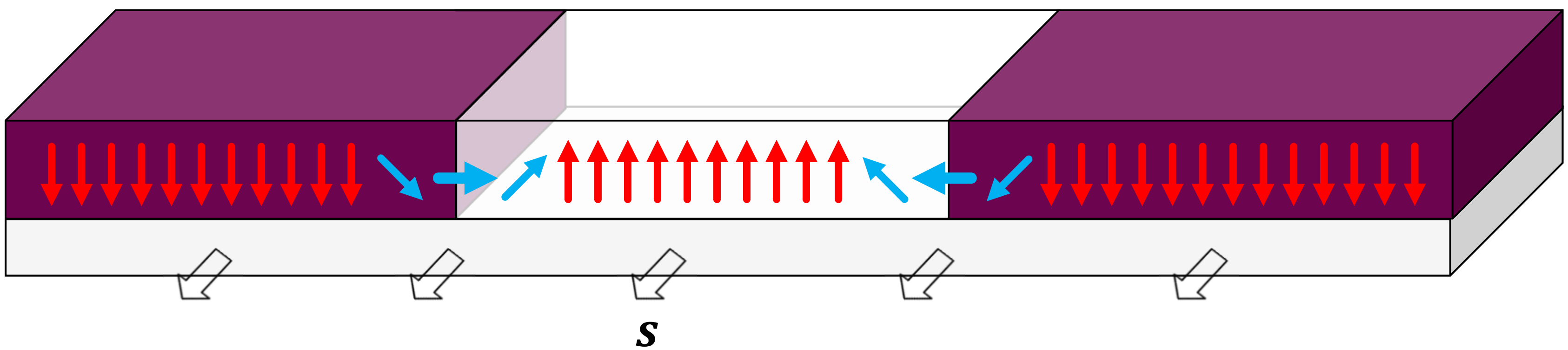

Spin-orbit torques acting on domain walls

Bloch walls

$$\boldsymbol{s} \parallel \boldsymbol{M}_{DW} \Rightarrow \boldsymbol{T}_{DL} = \boldsymbol{s} \times \boldsymbol{s} \times \boldsymbol{M}_{DW} = 0$$

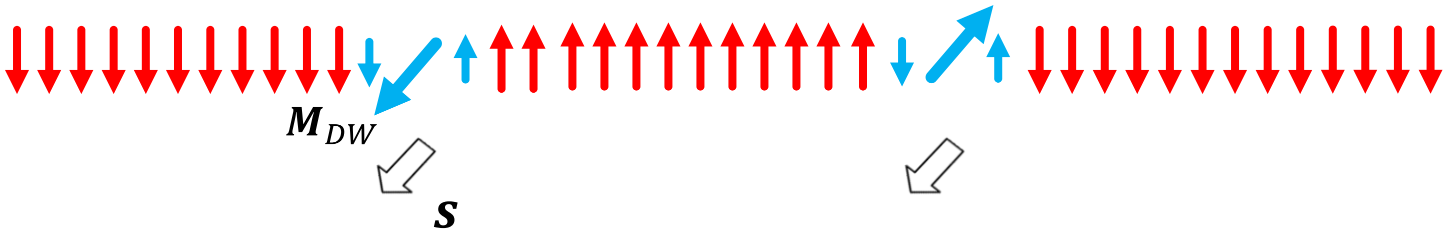

Néel walls

$$\boldsymbol{s} \perp \boldsymbol{M}_{DW} \Rightarrow \boldsymbol{T}_{DL} = \boldsymbol{s} \times \boldsymbol{s} \times \boldsymbol{M}_{DW} = max$$

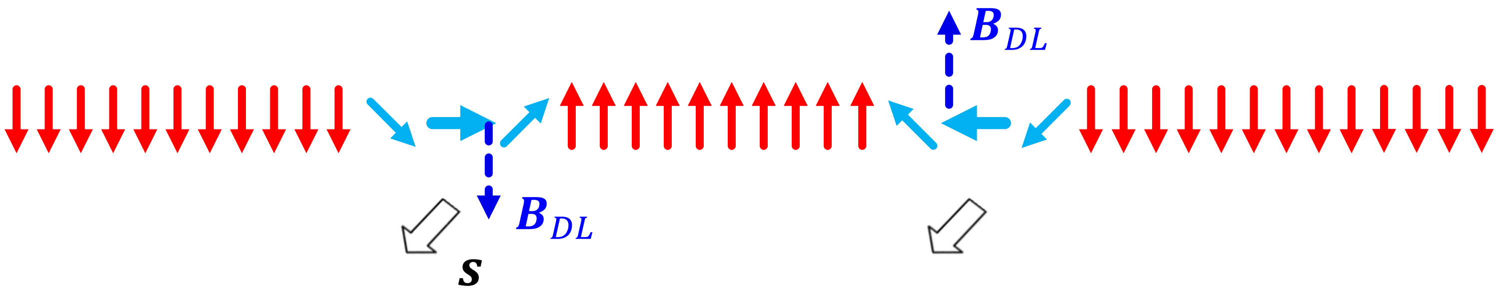

Thiaville et al., Europhys. Lett. **100**, 57002 (2012); Khvalkovskiy et al., PRB **87**, 020402R (2013)

Spin-orbit torque induced domain wall motion in magnetic racetracks

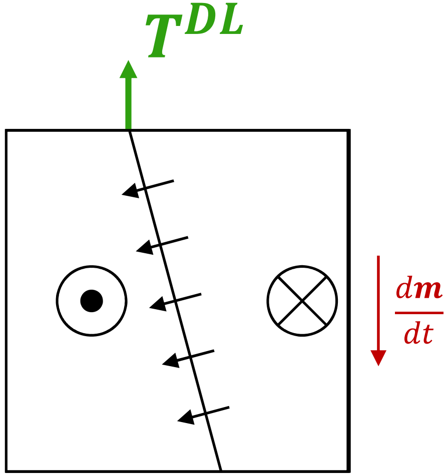

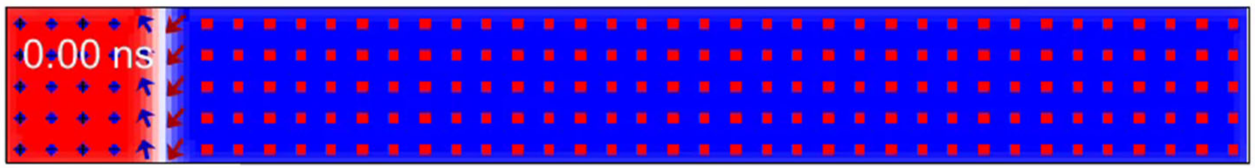

$j = 2 \cdot 10^8\ A\ cm^{-2}$ ($T^{DL} = 36$ mT)

Baumgartner & PG, APL **113**, 242402 (2018)

Miron et al., *Nat. Mater*. 2011; Thiaville et al., *Europhys. Lett*. 2012

Ryu et al. *Nat. Mater*. 2013; Emori et al., *Nat. Mater*. 2013

Chiral domain walls due to interfacial DMI in thin films with PMA

$$\mathcal{H}_{DMI} = -\boldsymbol{D} \cdot \boldsymbol{S}_1 \times \boldsymbol{S}_2$$

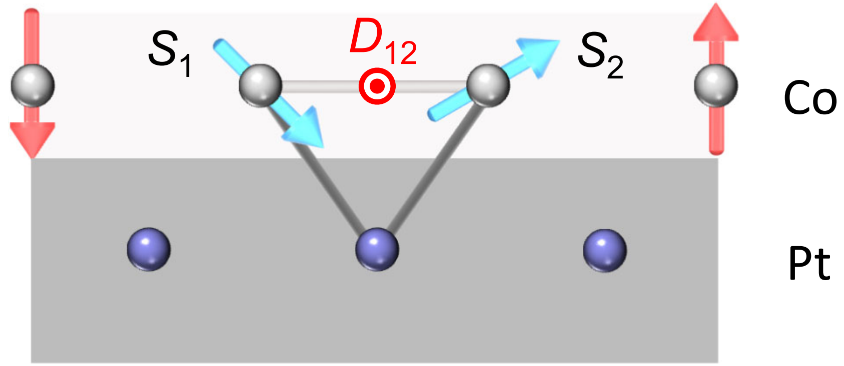

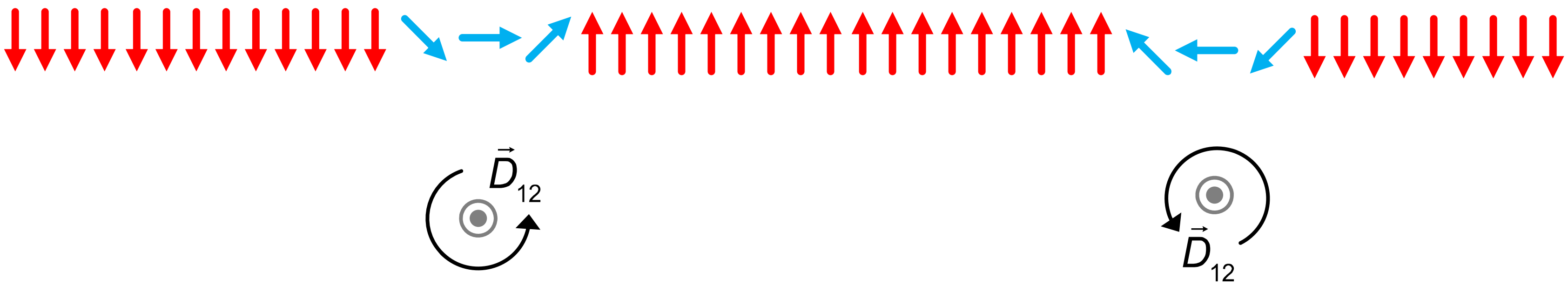

Fert and Levy, PRL **44**, 1538 (1980); Kubetzka et al., PRL **88**, 057201 (2002); Heide et al., PRB **78**, 140403 (2008)

Chiral domain walls measured by scanning NV magnetometry

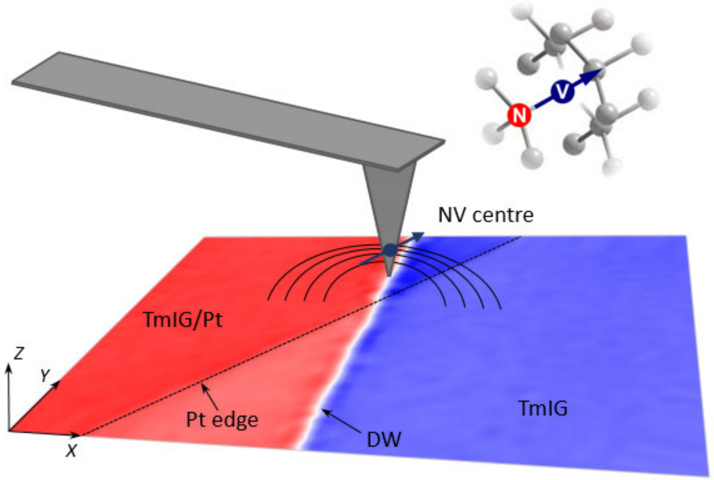

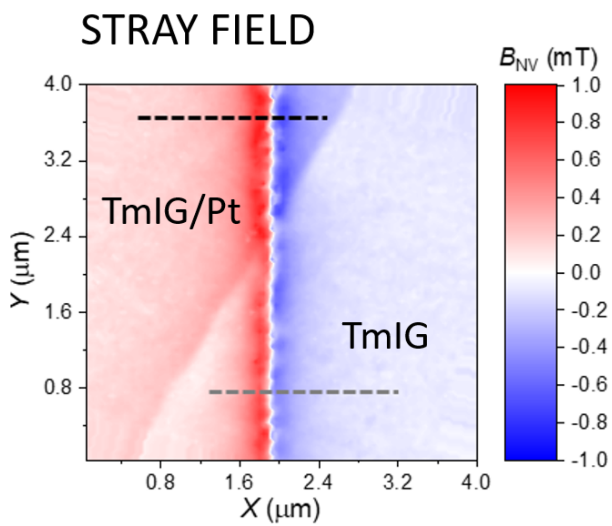

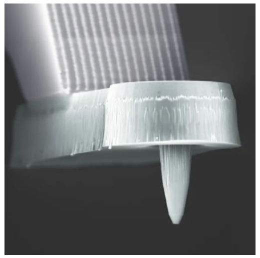

C. Degen
M. Wörnle
qzabre.com

QZABRE

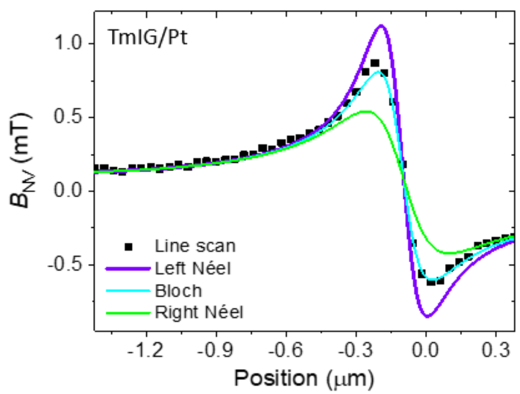

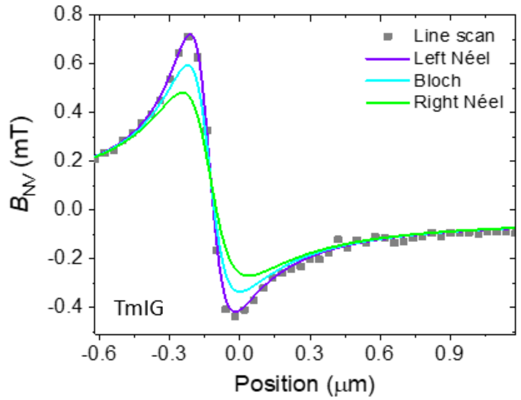

TmIG/Pt: Bloch/left Néel

TmIG: Left Néel

Vélez, PG et al., Nat. Comm. **10**, 4750 (2019)

Current-induced domain wall motion in a magnetic insulator

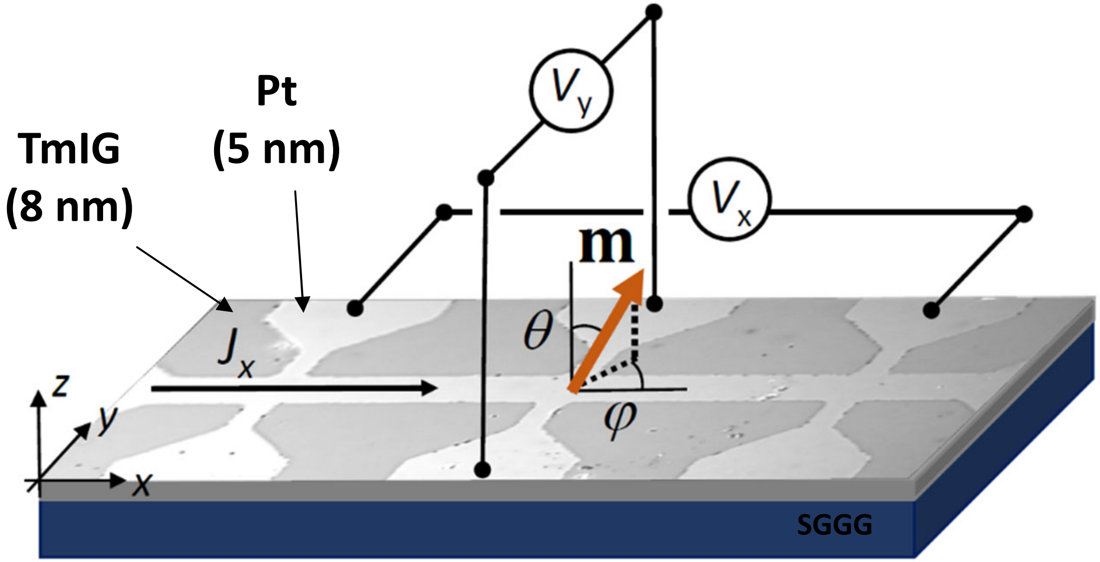

Vélez, PG et al., Nat. Comm. **10**, 4750 (2019)

Current-induced switching and domain wall motion in Pt/TmIG

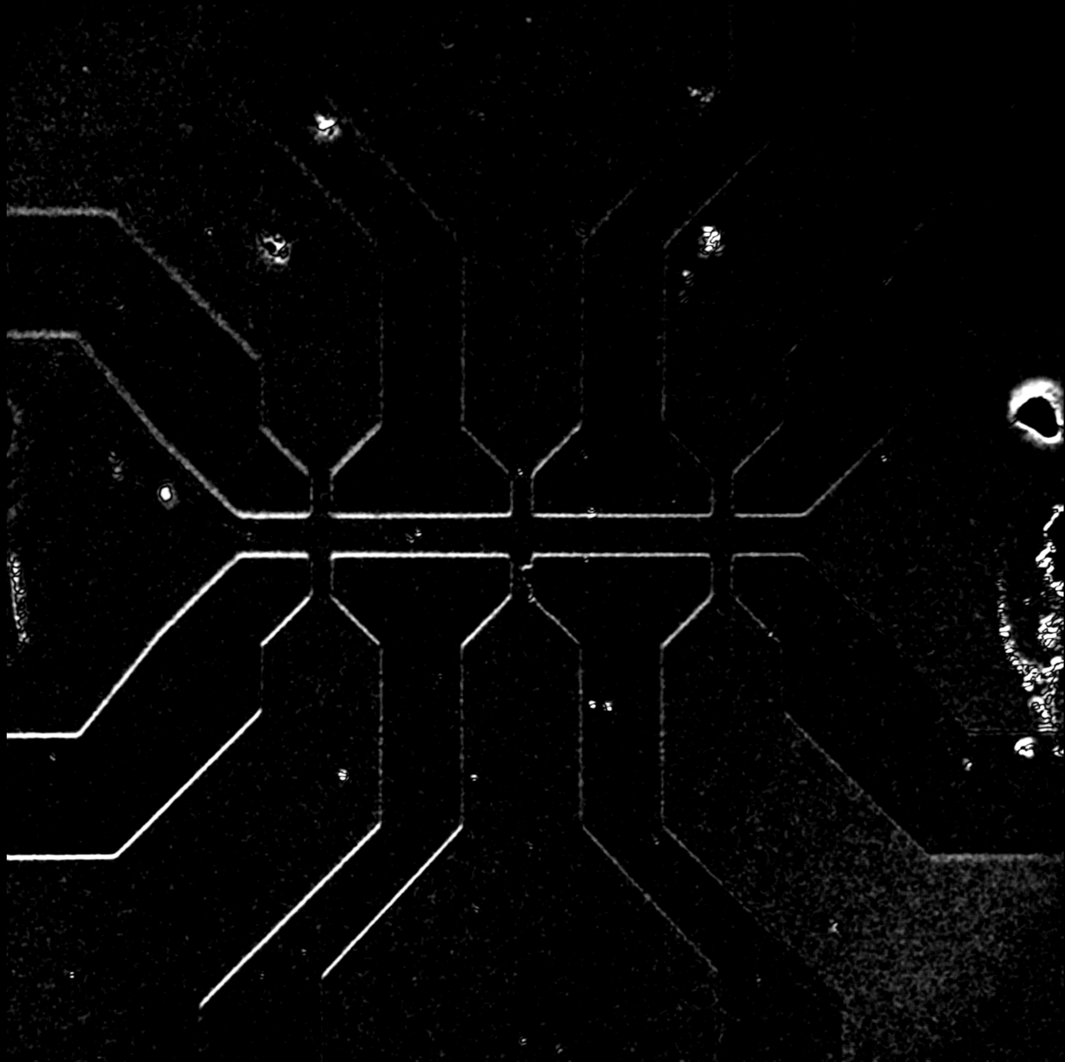

p-MOKE

J_x = 10^8 A cm^{-2}

t_p = 250 ns

H_x = 215 Oe

Vélez, PG et al., Nat. Comm. **10**, 4750 (2019)

Current-induced switching and domain wall motion in Pt/TmIG

p-MOKE

J_x = -10^8 A cm^{-2}

t_p = 250 ns

H_x = 215 Oe

Vélez, PG et al., Nat. Comm. **10**, 4750 (2019)

Current-driven stabilization of skyrmion bubbles in Pt/TmIG/YIG

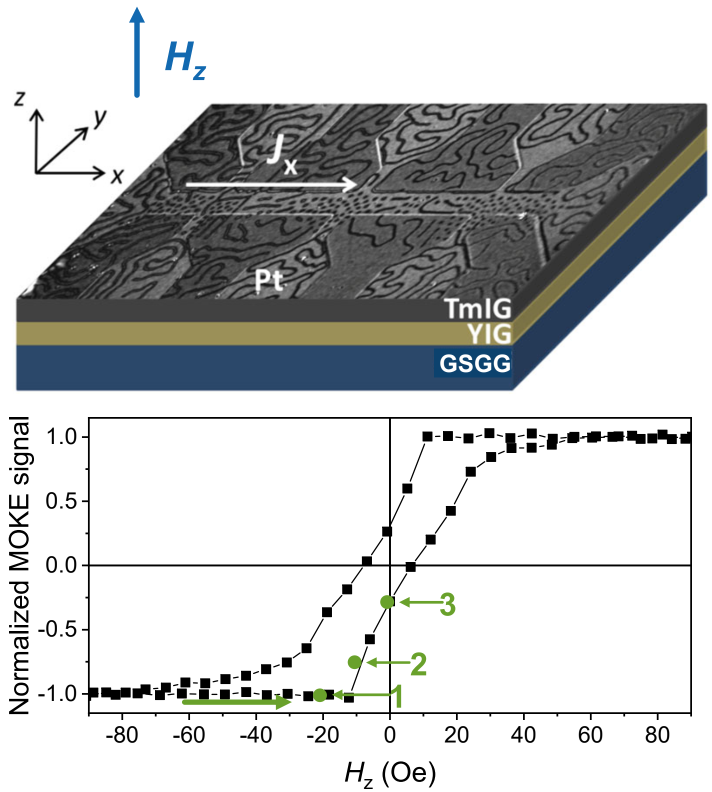

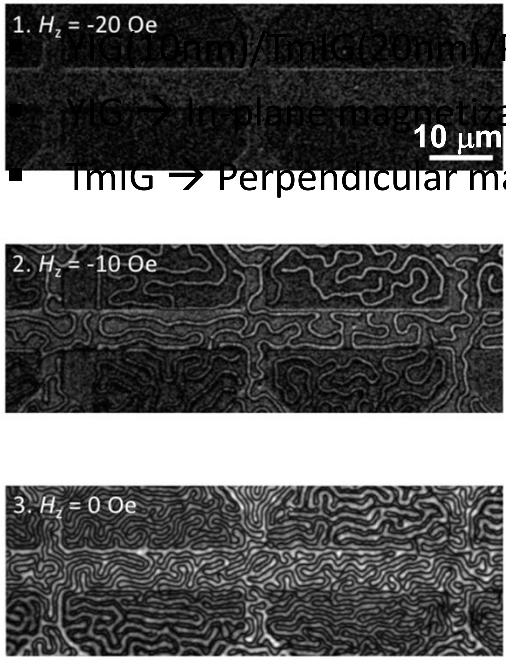

- YIG(10nm)/TmIG(20nm)/Pt(5nm) on GSGG
- YIG → In-plane magnetization
- TmIG → Perpendicular magnetization

- YIG is demagnetized

- Current pulses can nucleate bubble domains and break stripe domains into bubble domains

Vélez et al., Nat. Nanotech. **17**, 834 (2022)

NV magnetometry of skyrmions in Pt/TmIG/YIG

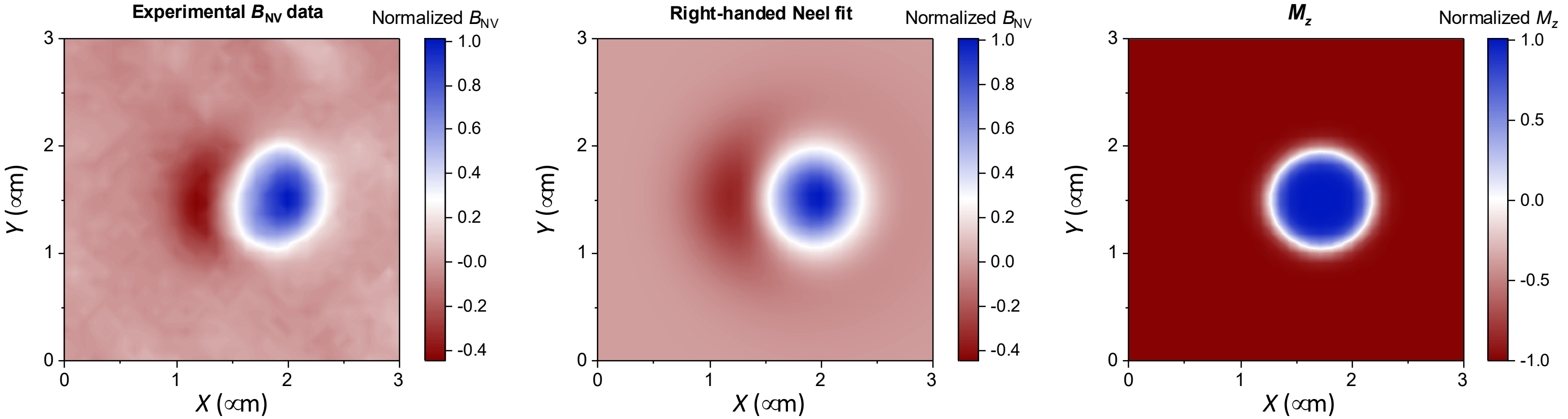

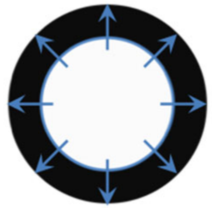

Right-Néel

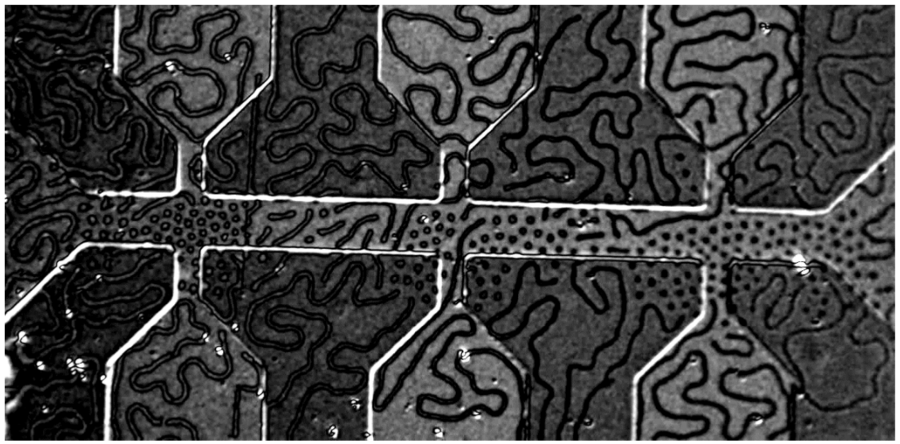

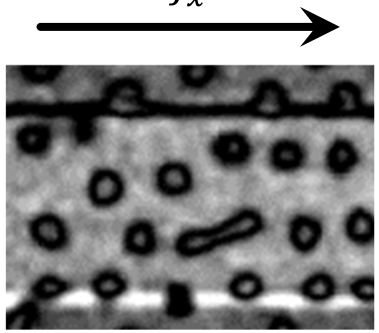

$|J_x|$~ 7x10^{11} A m^{-2}
t_p= 50 ns
H_z = -10 Oe
1 pulse/frame

Vélez et al., Nat. Nanotech. **17**, 834 (2022)

Current-driven skyrmions in YIG/TmIG/Pt

Skyrmion Hall effect

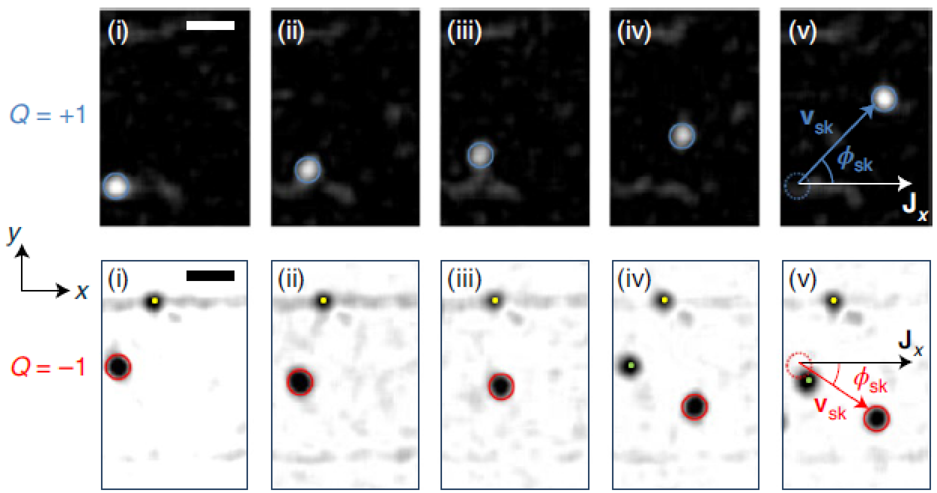

$$\phi_{\rm sk} \approx \tan^{-1}\left(-\frac{s_{\rm net}}{s_{\rm tot}}\frac{2\Delta_{\rm DW}Q}{\alpha R}\right)$$

Hopping motion

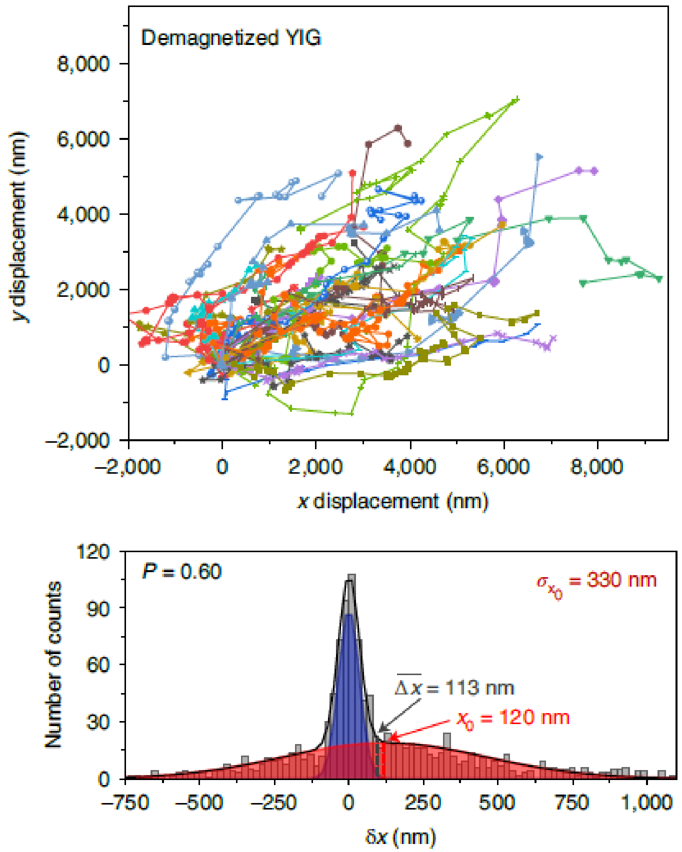

Vélez et al., Nat. Nanotech. **17**, 834 (2022)

From chiral Néel walls to chirally-coupled nanomagnets

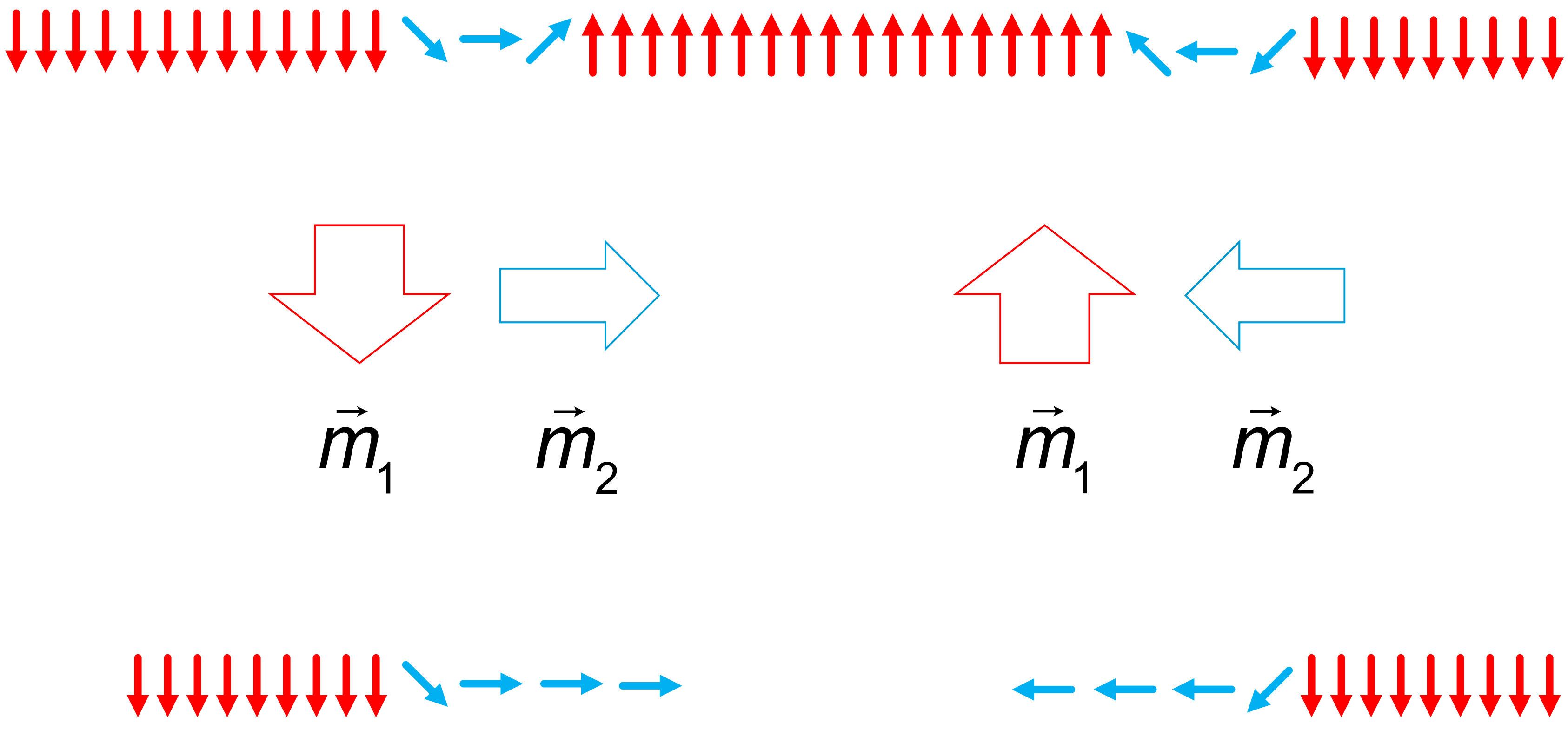

$$H_{DM} = -\vec{D}_{12} \cdot (\vec{m}_1 \times \vec{m}_2)$$

From chiral walls to chirally-coupled nanomagnets

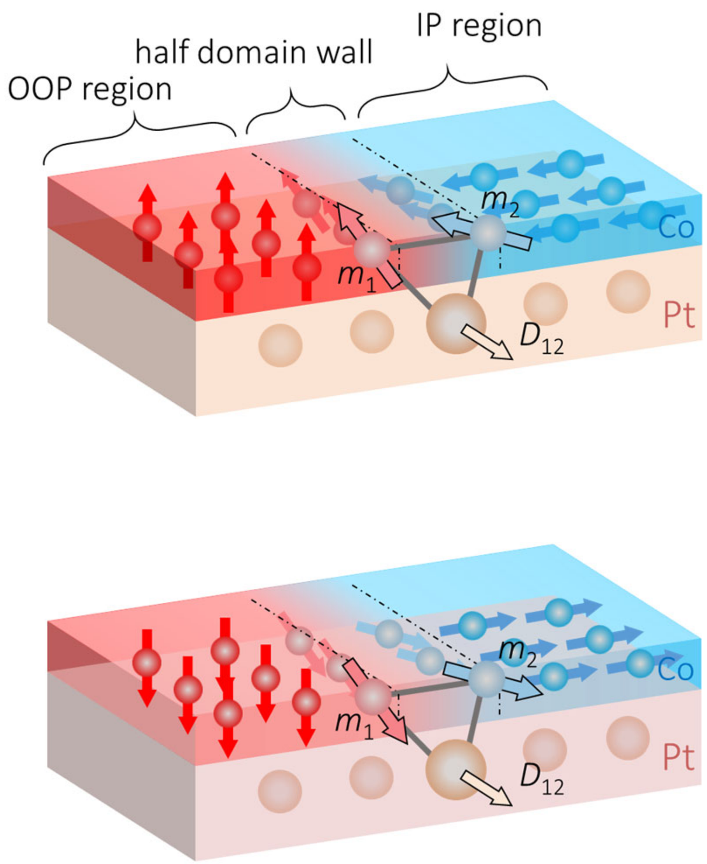

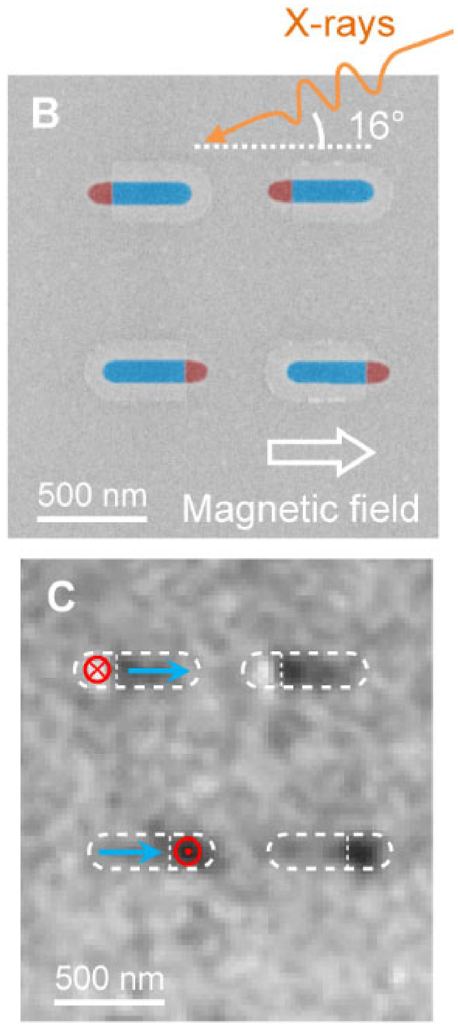

XPEEM @ SIM beamline/PSI

Luo, Dao, Hrabec, Heyderman, PG et al., Science **363**, 1435 (2019)

ETH zürich

DMI-induced lateral coupling

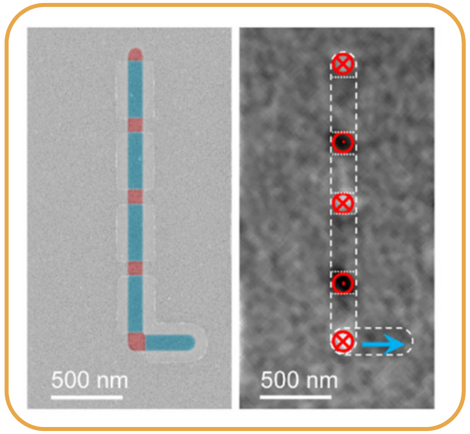

planar synthetic antiferromagnets

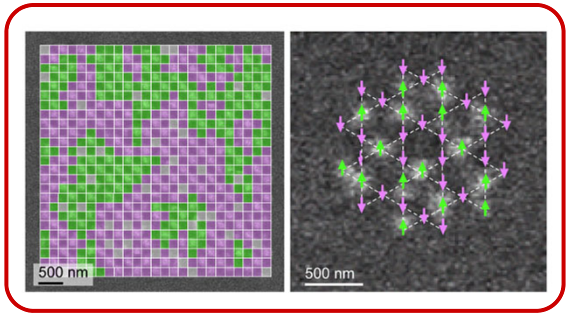

artificial spin ices

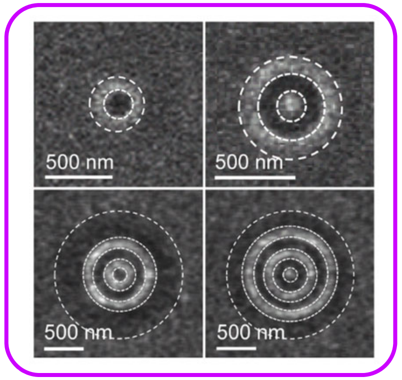

synthetic skyrmions

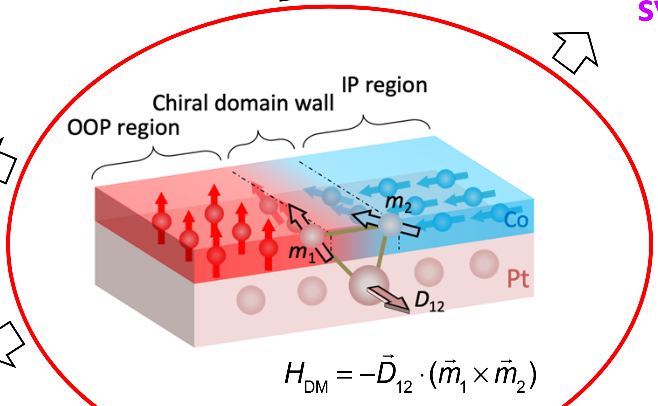

chiral coupling

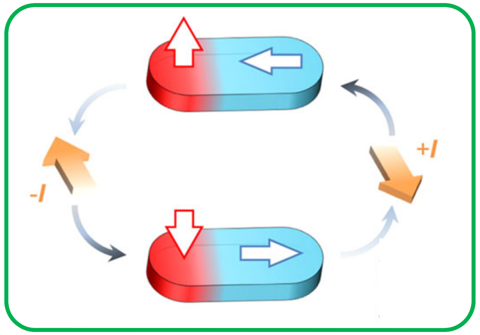

field-free SOT switching

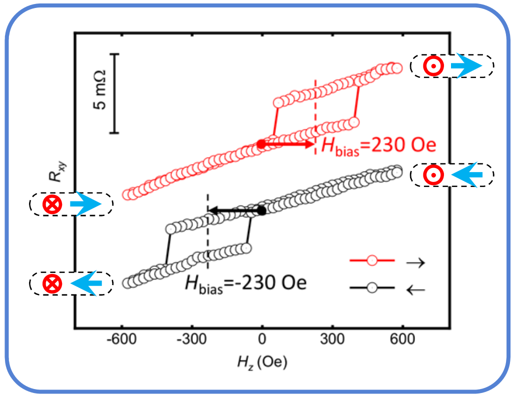

lateral exchange bias

Luo et al.,
Science **363**, 1435 (2019)
Dao et al.,
Nano Lett. **19**, 5930 (2019)
Hrabec et al.,
APL **117**, 130503 (2020)

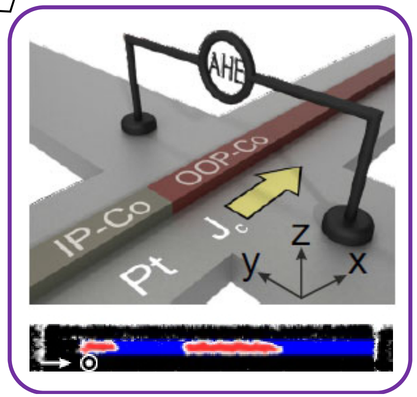

domain wall injector

Current-driven domain-wall inverter

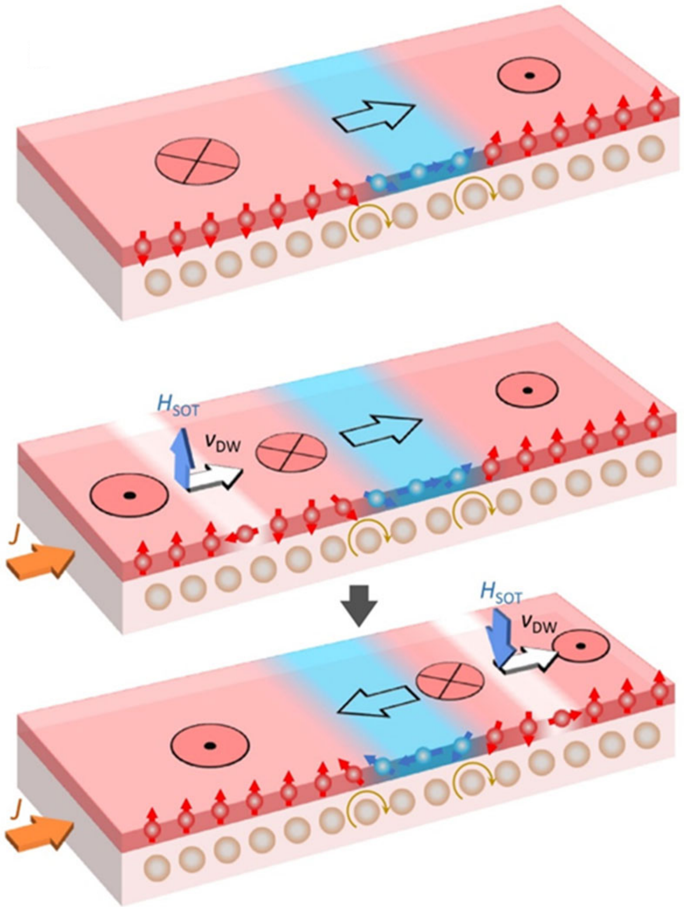

Z. Luo, et al., *Nature* **579**, 214 (2020)

Experiment

STXM measurement of an OOP-IP-OOP racetrack

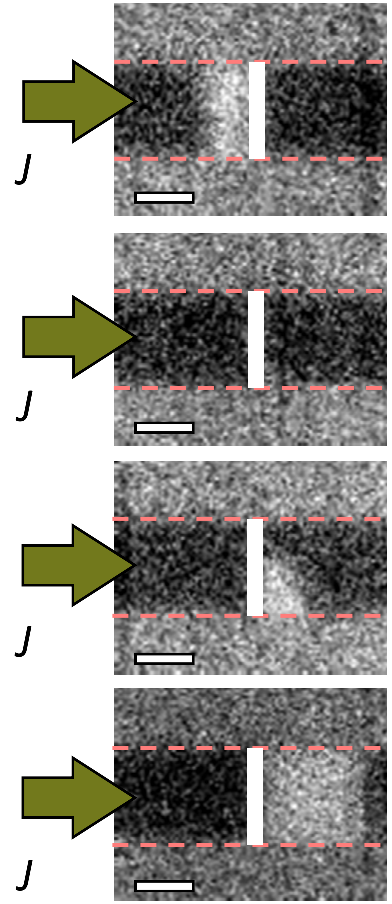

The ⊗|⊙ DW is inverted into a ⊙|⊗ DW by the current pulses

Domain-wall NOT gate

We define ⊗ = logical ‘1’ and ⊙ = logical ‘0’

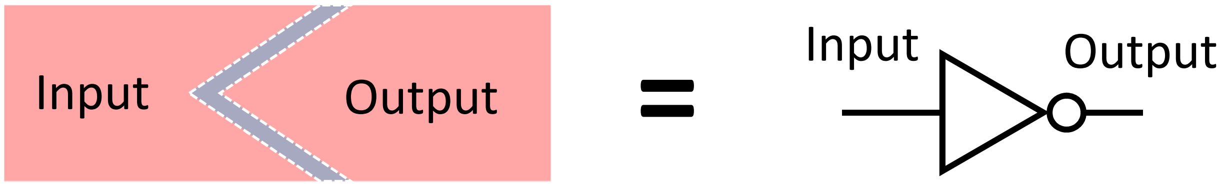

Data flow

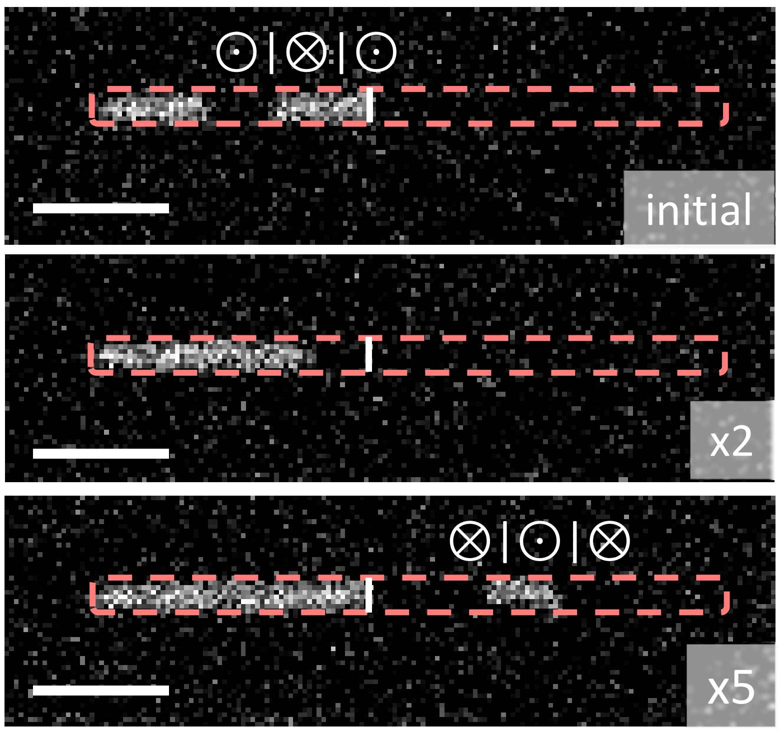

Cascaded NOT gates

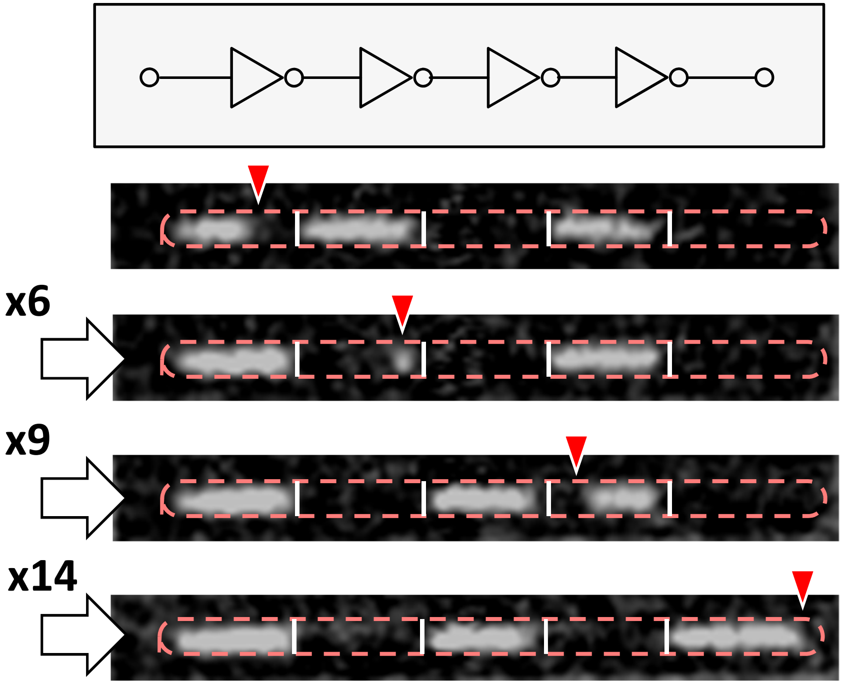

Fabricating majority logic gates based on DMI coupling

DW reservoir w/wo inverter to define inputs

Computation core based on chiral coupling

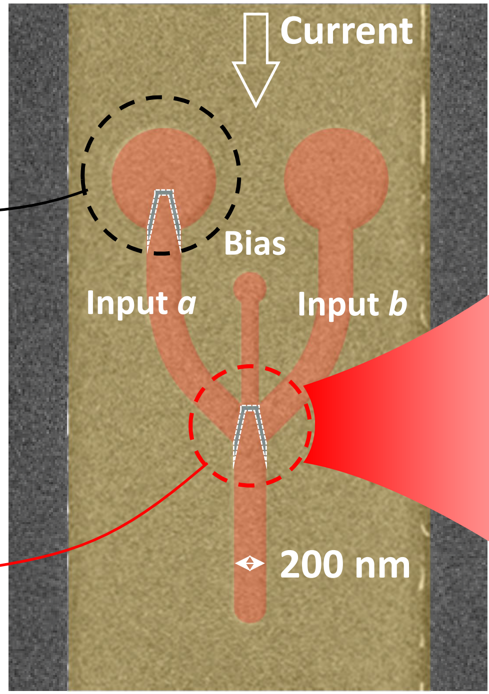

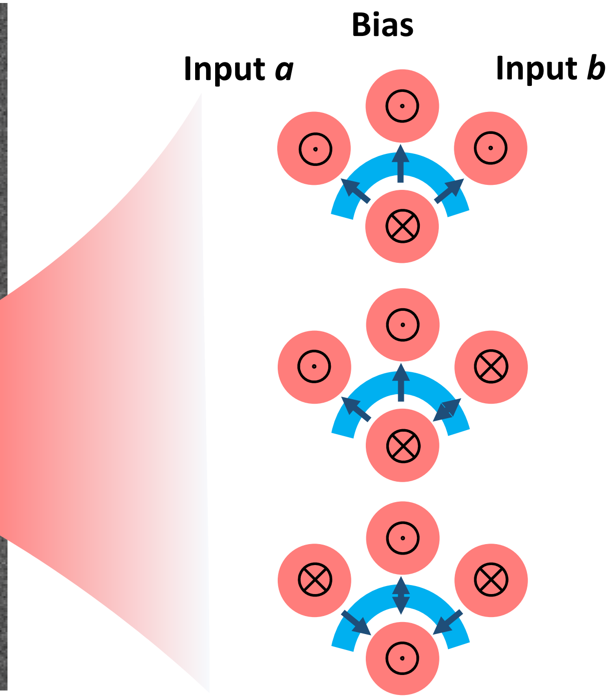

Luo, Hrabec, Heyderman, PG et al., *Nature* **579**, 214 (2020)

ETH zürich

Examples of DW logic circuits enabled by SOT and chiral coupling

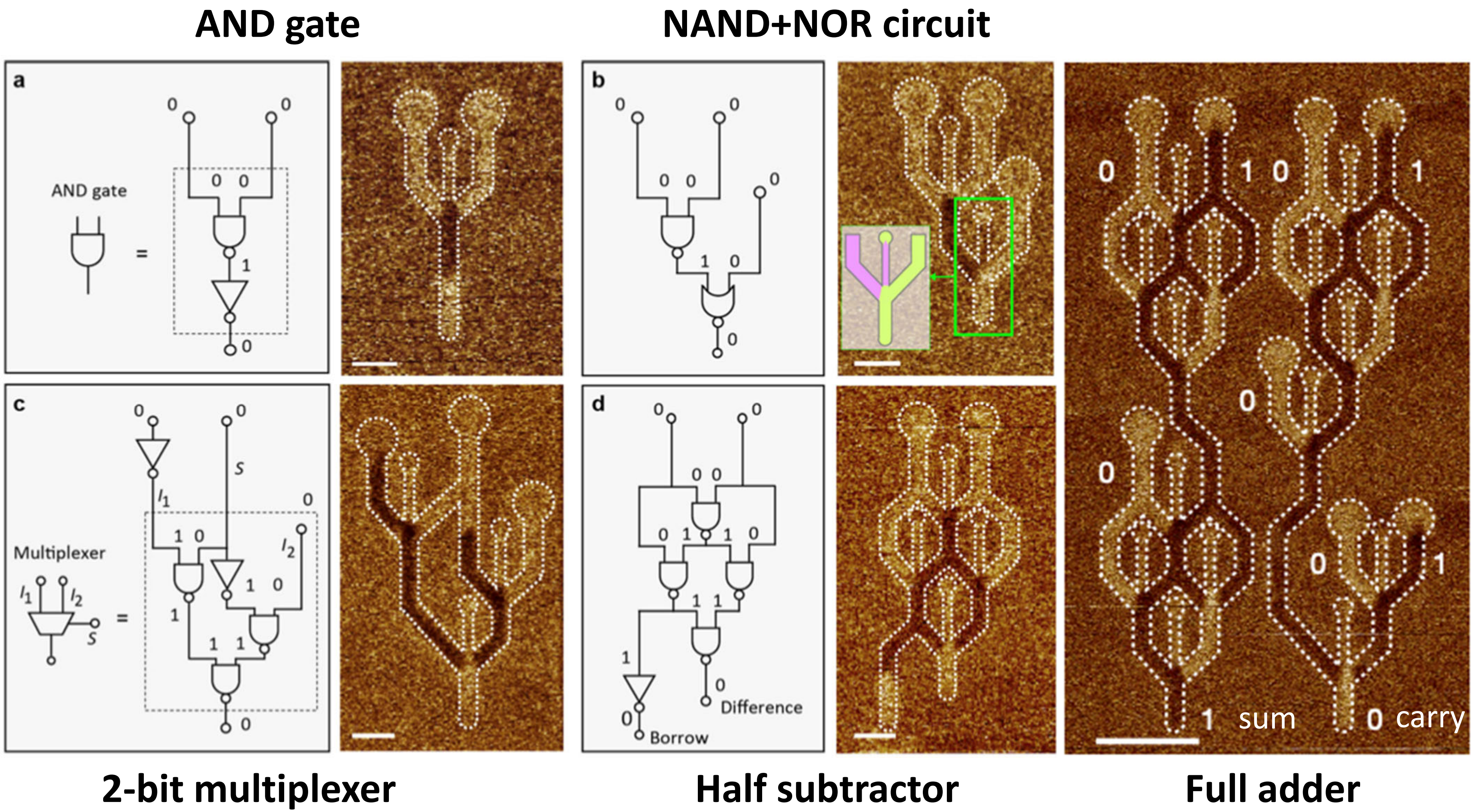

Luo, Hrabec, Heyderman, PG et al., *Nature* **579**, 214 (2020)

Spin-orbit torque switching of a single ferromagnetic layer

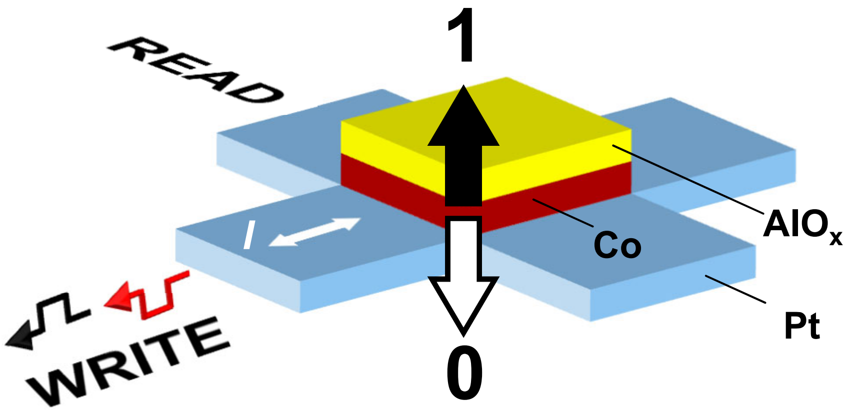

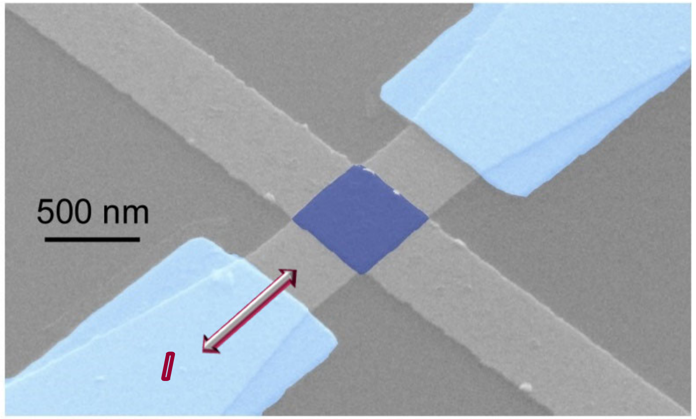

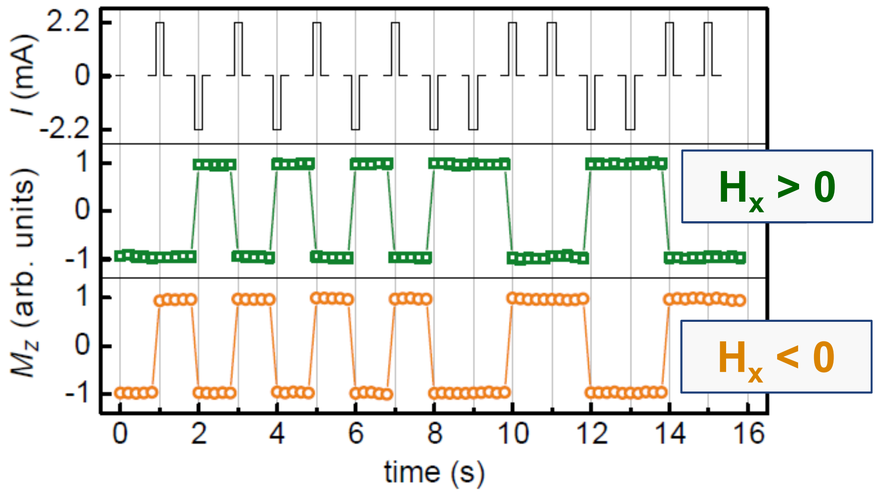

- ✓ Transfer of *orbital* to *spin* momentum
- ✓ Efficient spin injection/No polarizer
- ✓ Scalable
- ✓ Versatile (PMA, IMA, …)
- ✓ CMOS-compatible

Miron et al., *Nature* **476**, 189 (2011)

- DL torque is in-plane: switching of M_z requires symmetry-breaking field

Spin-orbit torque switching of a chiral antiferromagnets: Mn_3Sn

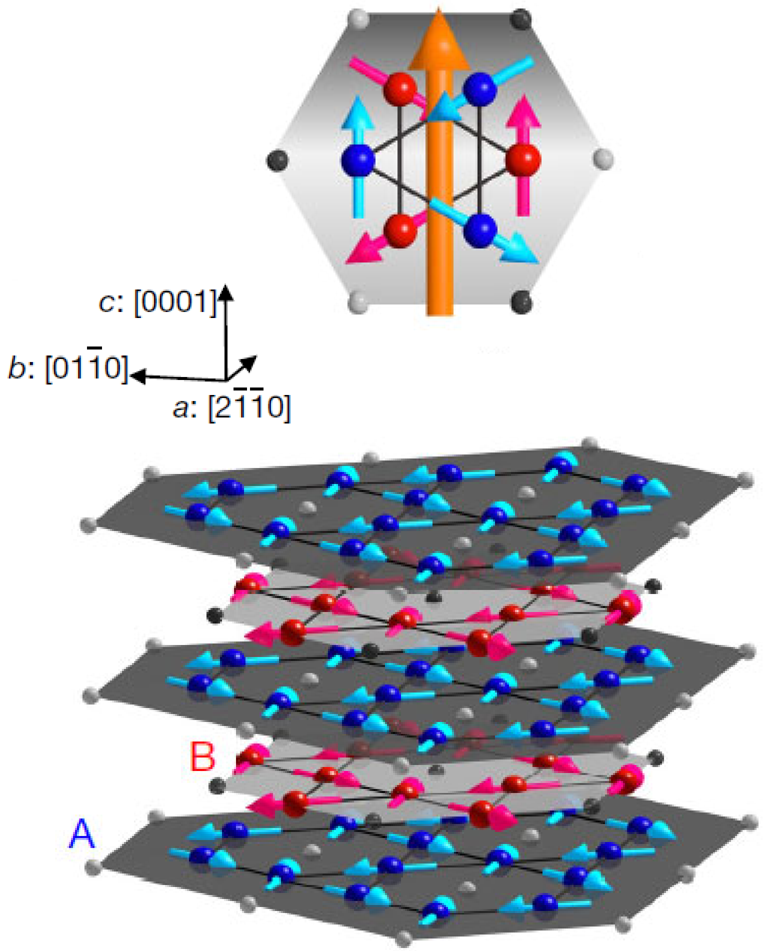

Nakatsuji et al., Nature 527, 212 (2015)

Tsai et al., Nature **580**, 608 (2020)

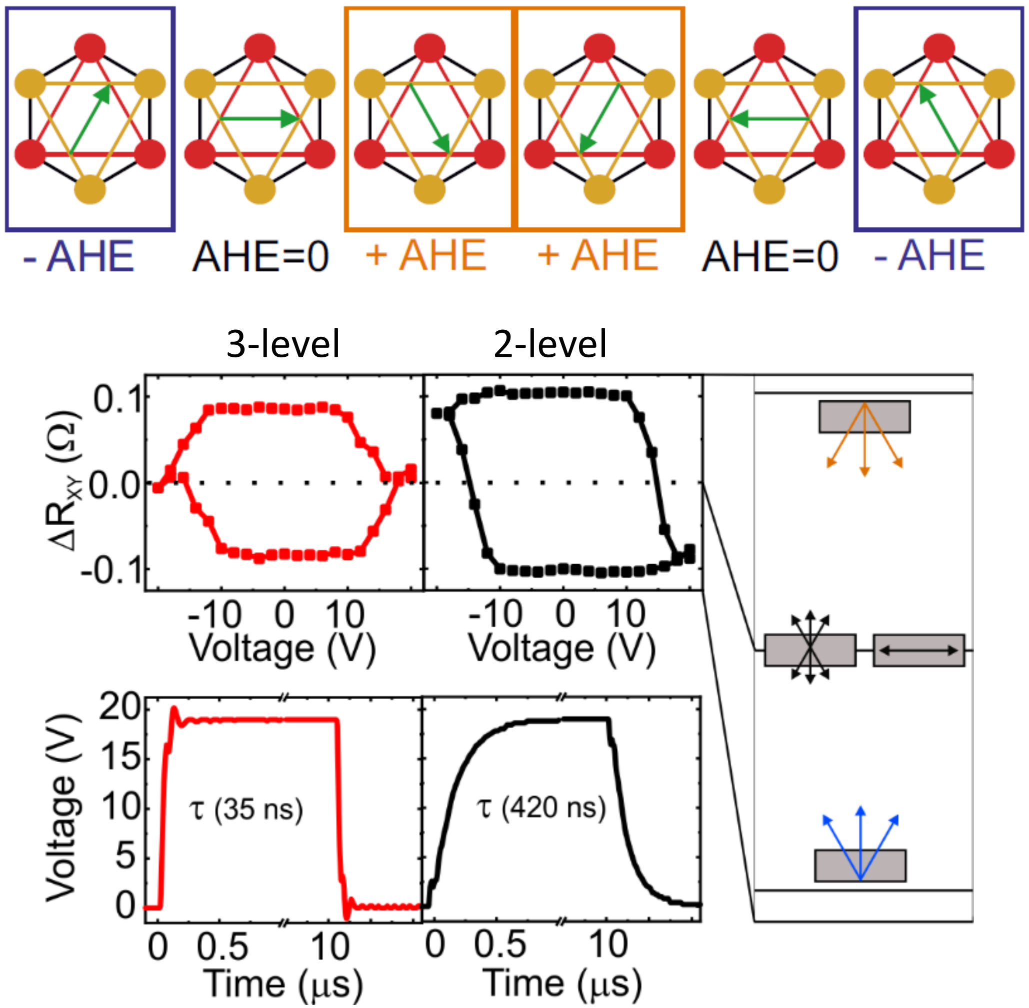

Krishnaswamy, PG et al., Phys. Rev. Appl. **18**, 024064 (2022)

Rare-earth transition-metal ferrimagnetic alloys

RE_xTM_{1-x}

GdFeCo, TbCo, DyCo, ...

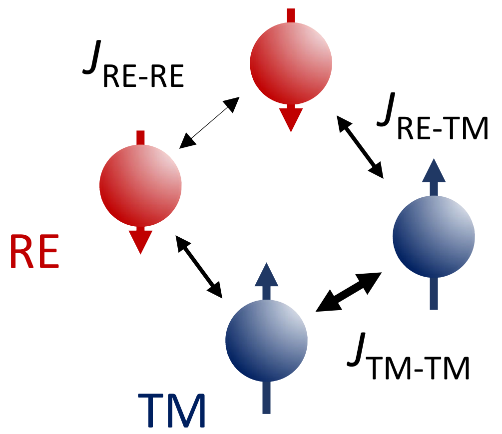

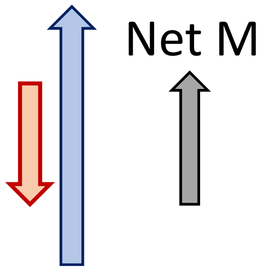

- Fast dynamics
- Easier to measure than AFMs
- Bulk PMA and DMI
- Low stray field
- Tunable by composition and temperature

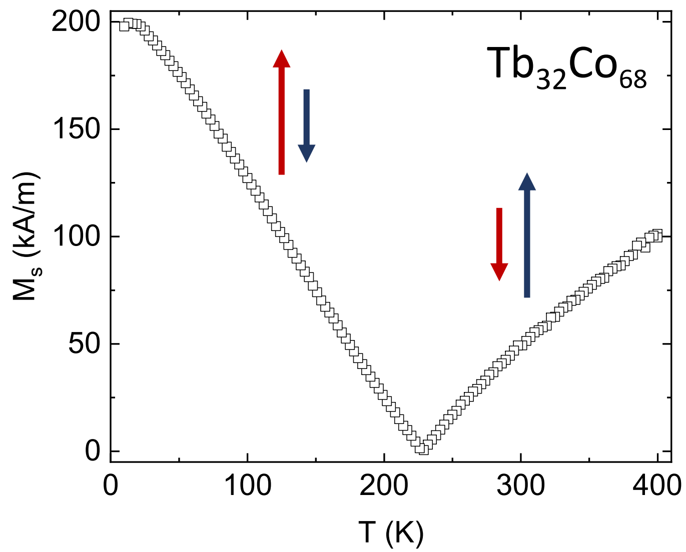

see, e.g., Buschow, Rep. Prog. Phys. **40**, 1179 (1977); Kim et al., Nat. Mater. **21**, 24 (2022)

SOT-induced switching of Pt(5 nm)/$Gd_{30}Fe_{63}Co_7$(15 nm) dots

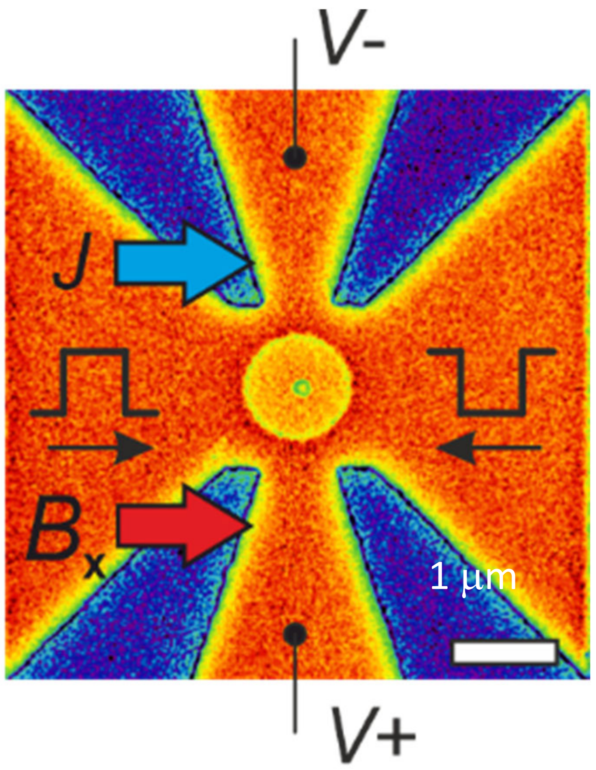

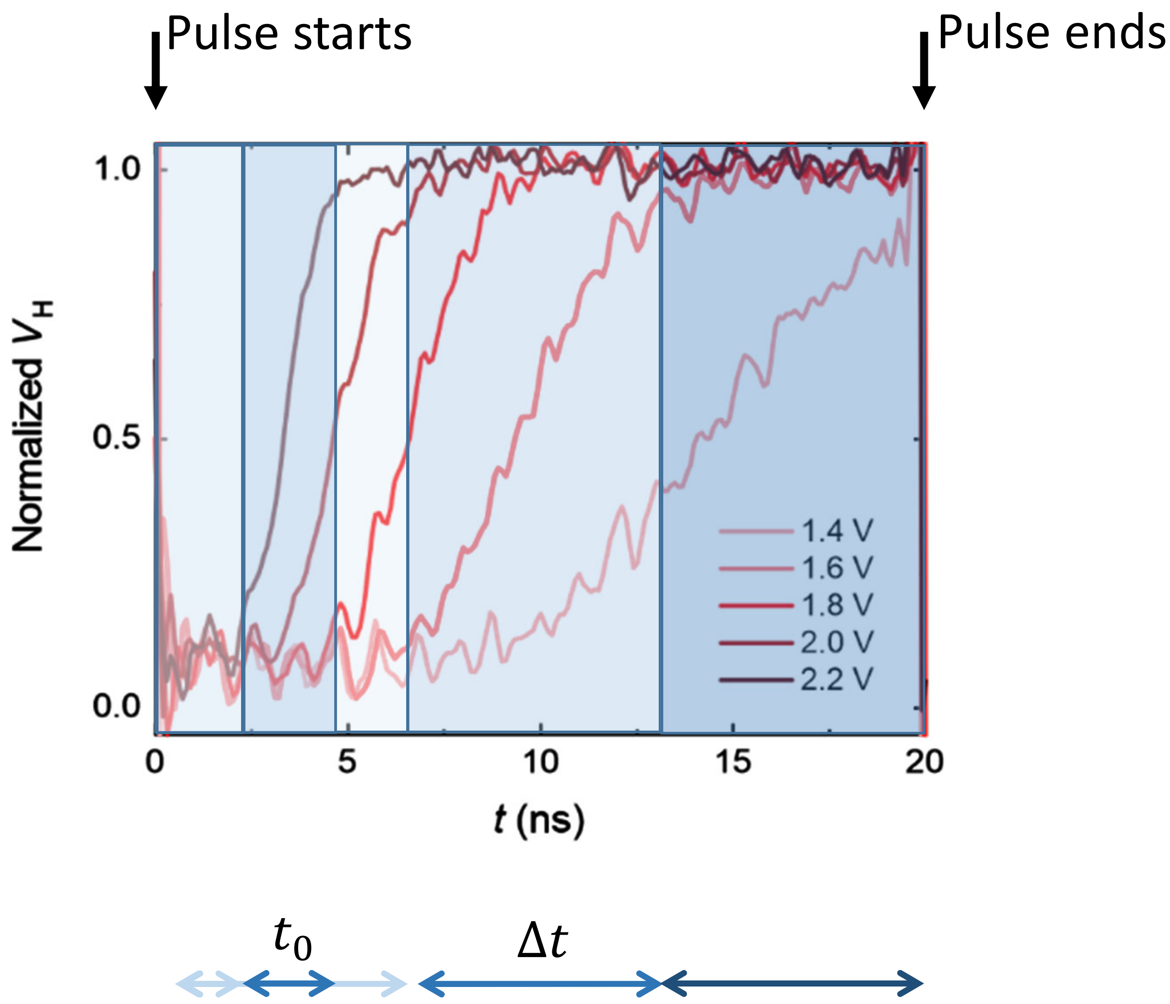

Sala et al., *Nat. Comm.* **12**, 656 (2021)

Time-resolved scanning transmission x-ray microscopy (STXM)

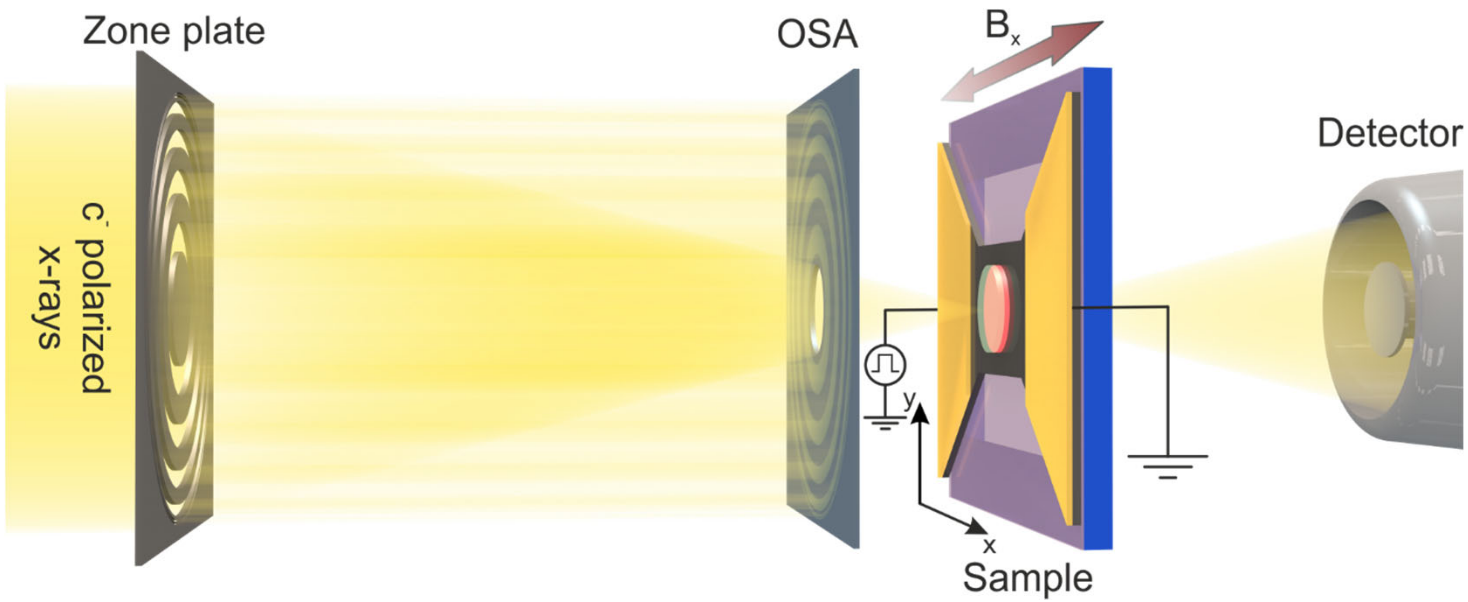

- Contrast due to XMCD
- Normal incidence: $\pm M_z$
- Element specific: Gd M_5-edge (1185eV)
  Fe L_3-edge (707 eV)
- Time resolution: $\sim 100\text{ ps}$
- Lateral resolution: $\sim 25\text{ nm}$

Current pump / x-ray probe measurements

- Pump: $0.8 - 20$ ns current pulses at 20 MHz rep rate
- Probe: 70 ps x-ray pulses at 500 MHz rep rate

PolLux beamline
Swiss Light Source

PAUL SCHERRER INSTITUT
PSI

Asynchronous switching of ferrimagnetic alloys

Type I

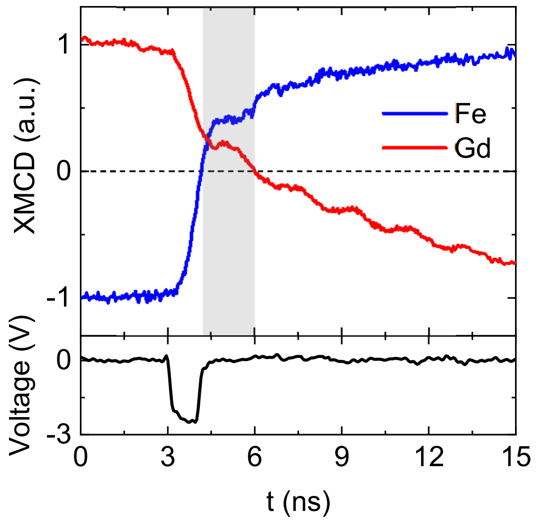

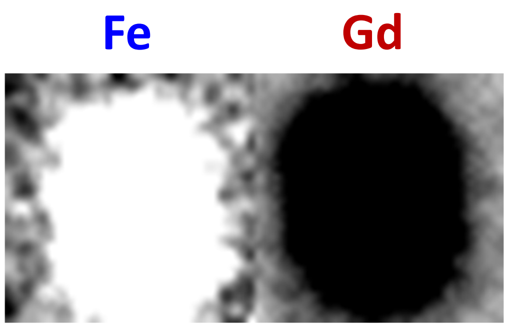

Sala et al., *Nat. Mater*. **21**, 640 (2022)

Asynchronous switching of ferrimagnetic alloys

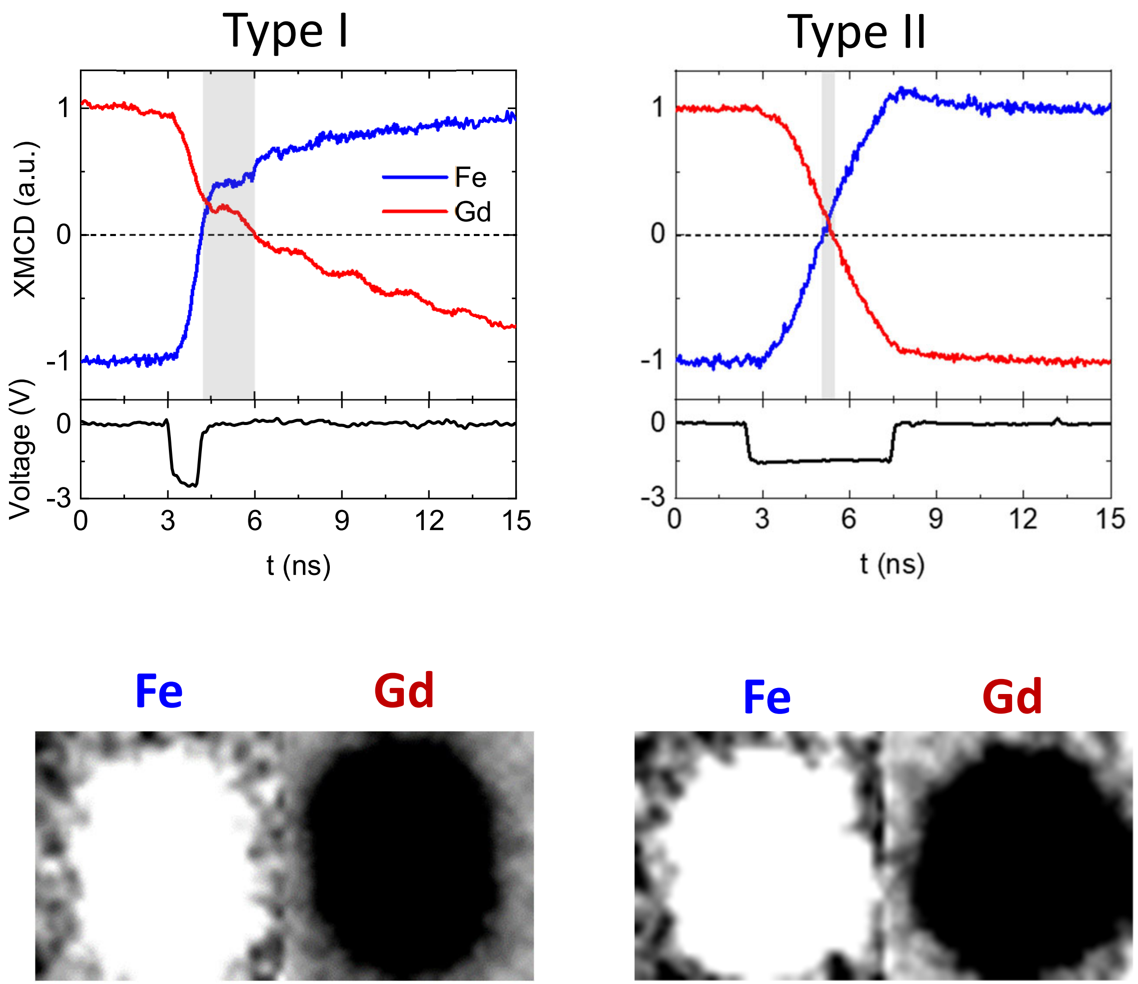

Sala et al., *Nat. Mater*. **21**, 640 (2022)

ETH zürich

Asynchronous and synchronous switching of ferrimagnetic alloys

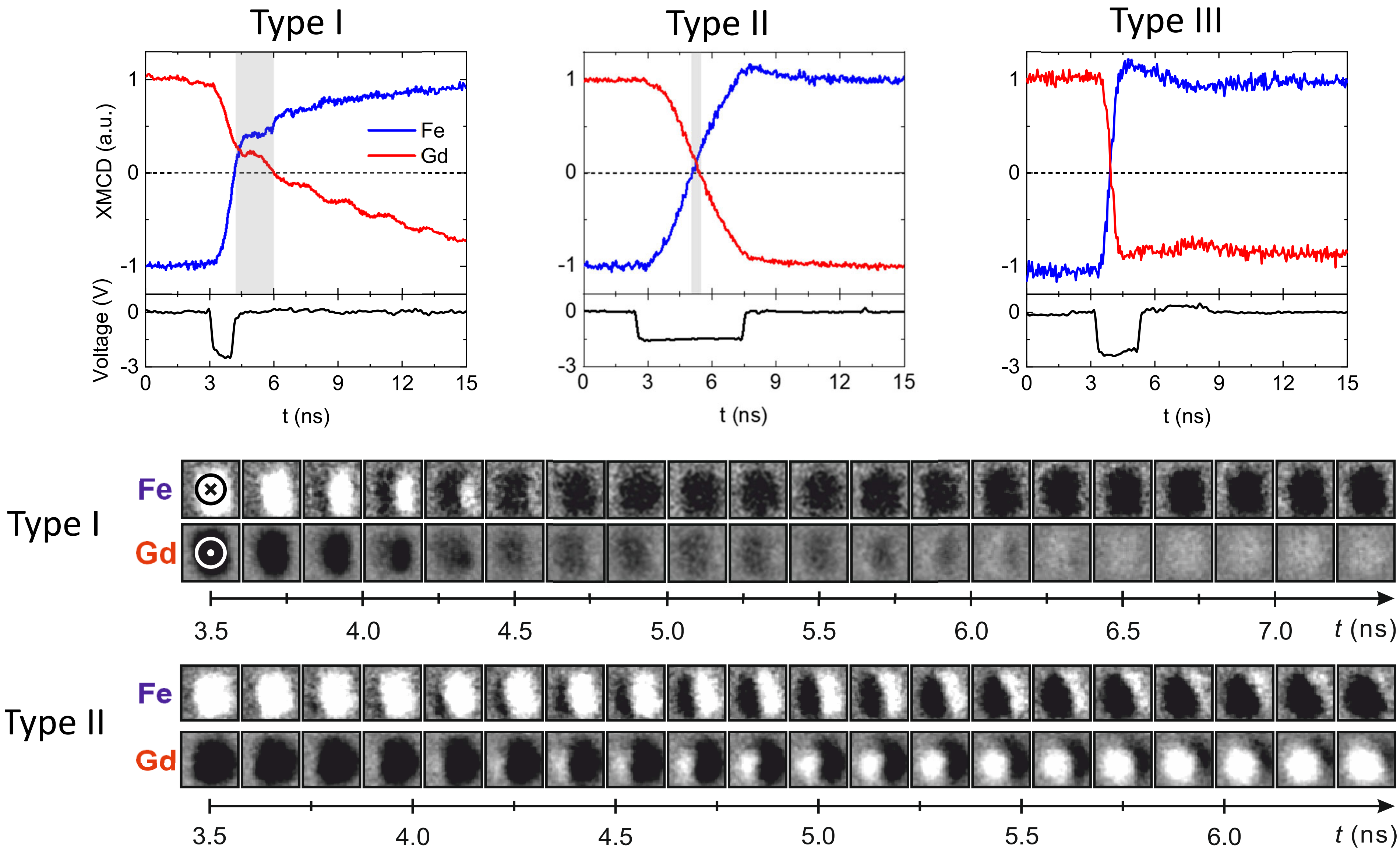

Sala et al., *Nat. Mater.* **21**, 640 (2022)

Switching of M_{TM} and M_{RE} in ferrimagnets

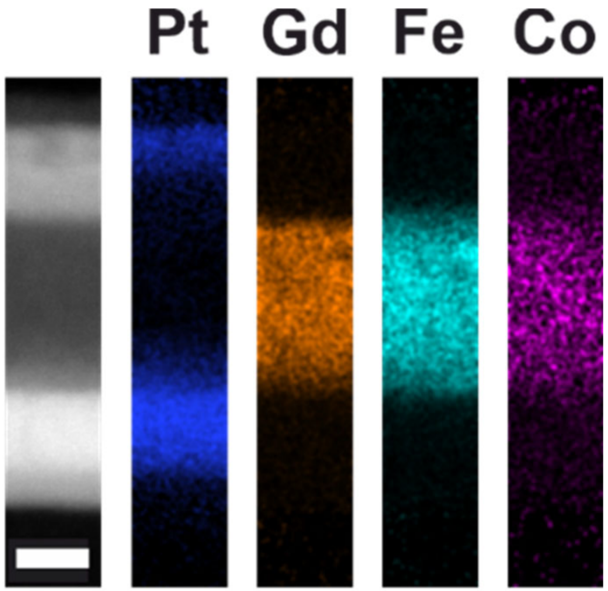

- Asynchronous switching of sublattice magnetizations with ns-long transient FM state
- Asymmetric action of spin-orbit torques on TM and RE sublattices: master-slave dynamics
- Variable strenght of antiferromagnetic coupling depending on alloy microstructure

G. Sala, E. Martinez, PG et al., *Nat. Mater*. **21**, 640 (2022)

Spin-orbit torque switching of binary MTJ devices

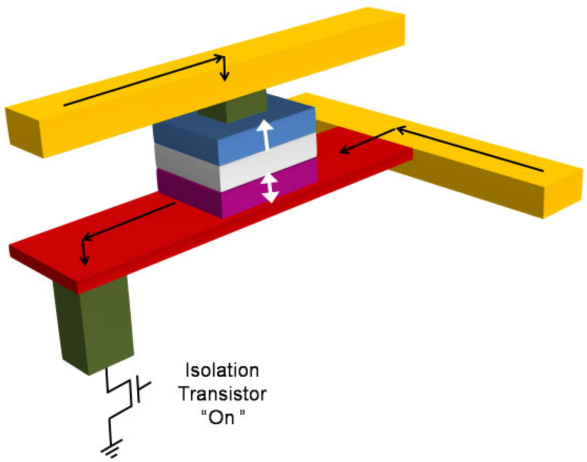

Perpendicular MTJ

Cubukcu et al.,
APL **104**, 042406 (2014)

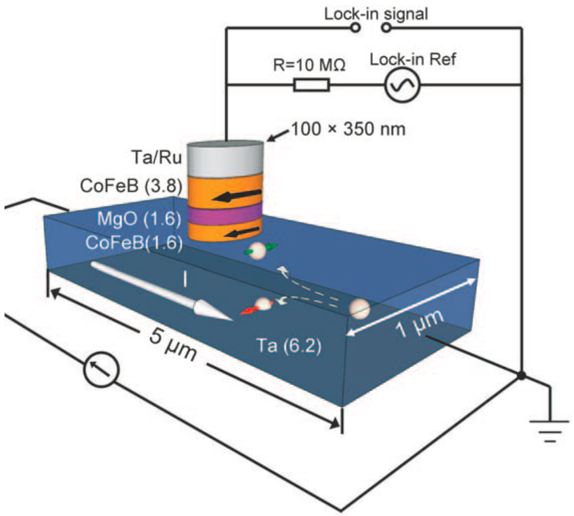

In-plane MTJ
“y-Type”

Liu et al.,
Science **336**, 555 (2012)

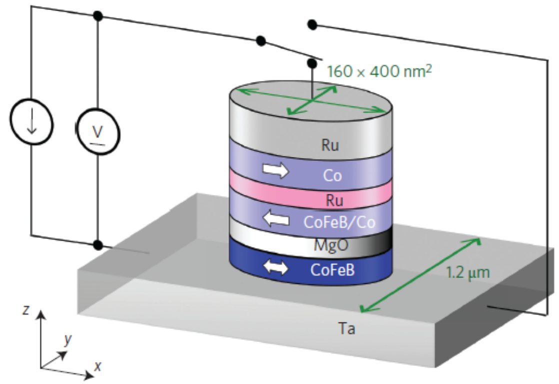

In-plane MTJ
“x-Type”

Fukami et al.,
Nat. Nano. **11**, 621 (2016)

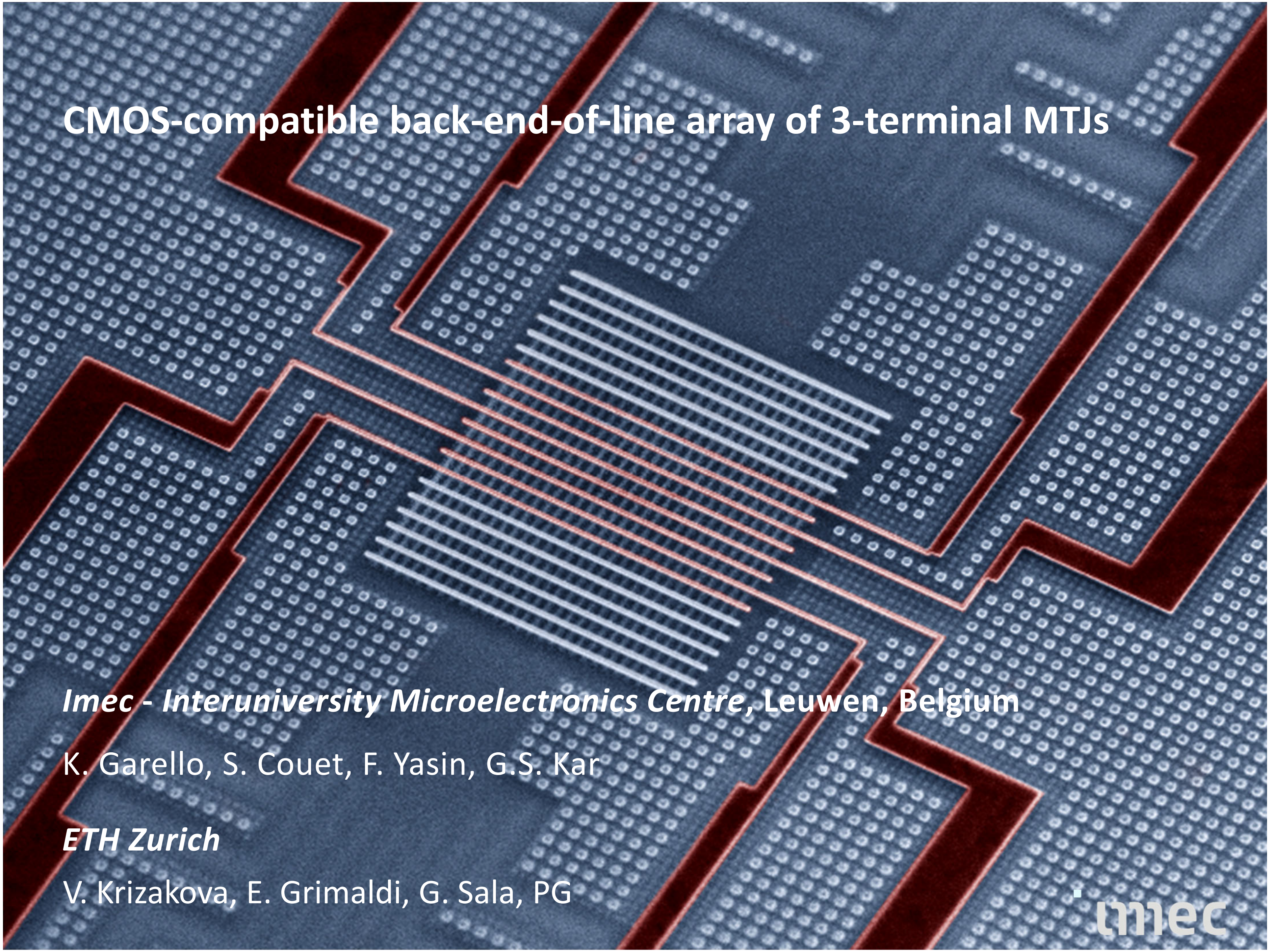

CMOS-compatible back-end-of-line array of 3-terminal MTJs

Imec - Interuniversity Microelectronics Centre, Leuwen, Belgium

K. Garello, S. Couet, F. Yasin, G.S. Kar

ETH Zurich

V. Krizakova, E. Grimaldi, G. Sala, PG

Dual pulse switching of 3-terminal MTJs

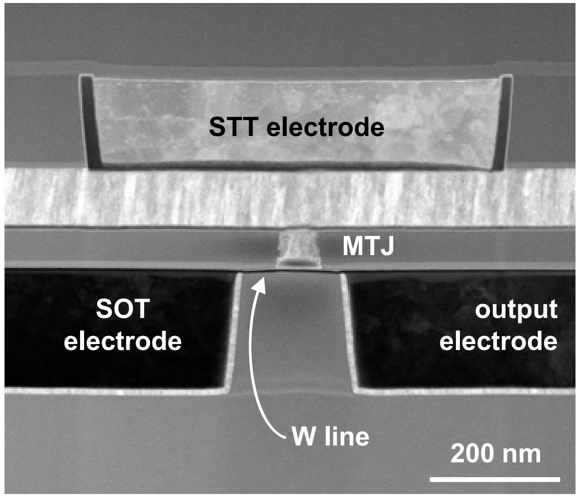

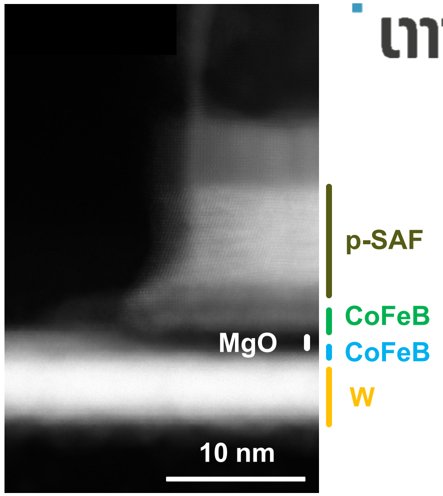

imec

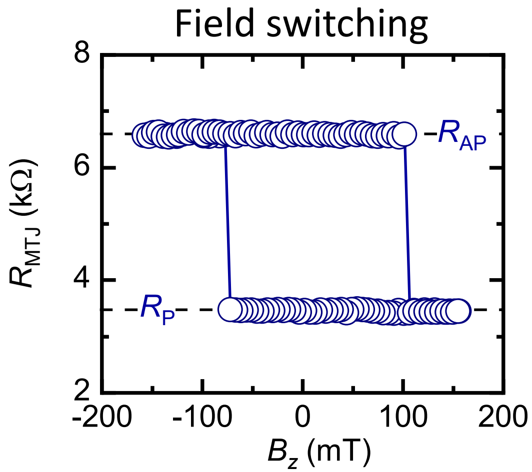

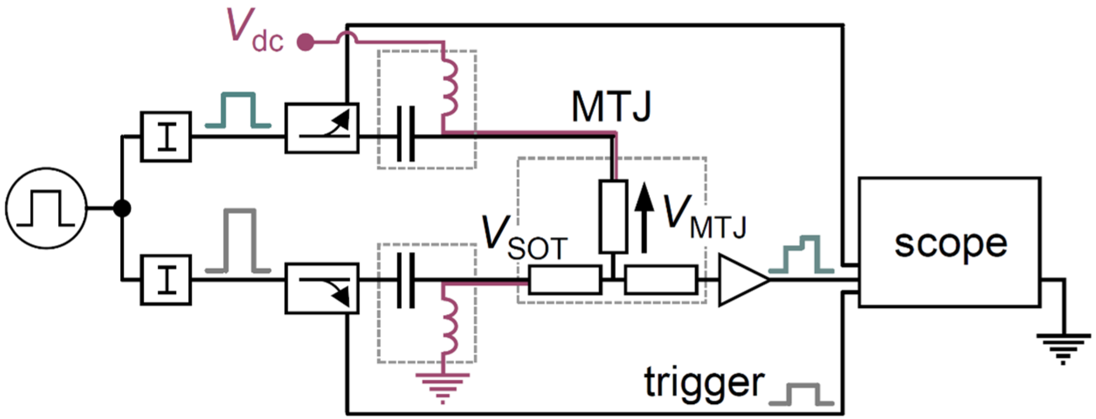

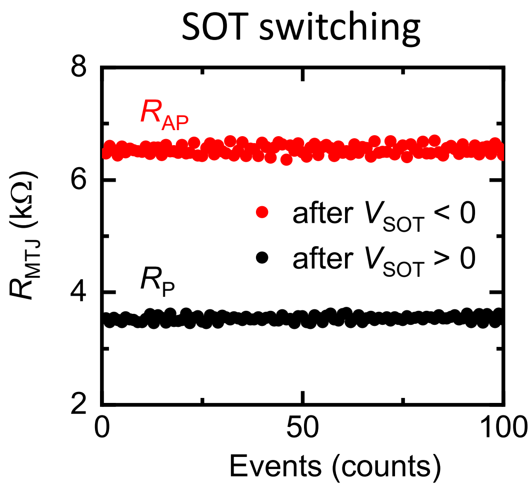

E. Grimaldi, V. Krizakova, K. Garello, PG et al., Nat. Nanotech. **15**, 111 (2020)

Single-shot SOT and STT switching in a 3T-MTJ

STT only

$V_{SOT} = 0$
$V_{STT} = +0.88\,V$

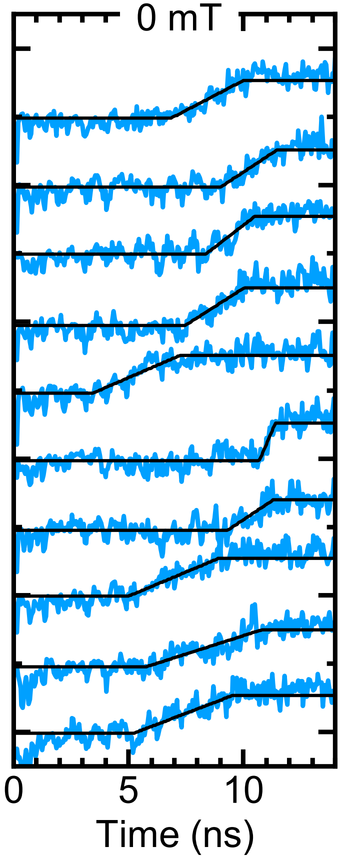

E. Grimaldi, V. Krizakova, K. Garello, PG et al., Nat. Nanotech. **15**, 111 (2020)

Squeezing the switching time distributions by VCMA, STT, self-heat

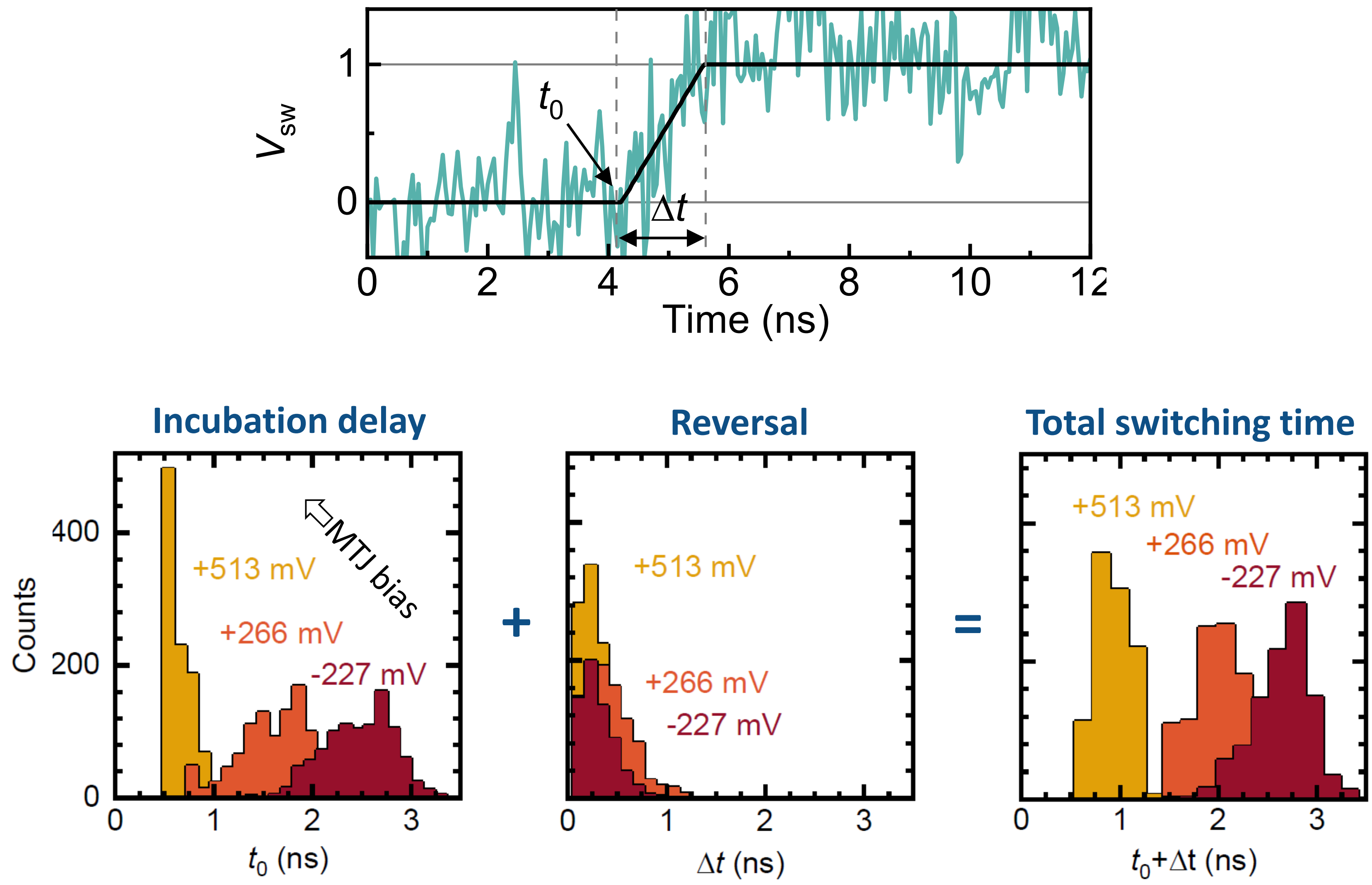

E. Grimaldi et al., Nat. Nanotech. **15**, 111 (2020)

Trade-off between speed and efficiency: comparison between STT and SOT

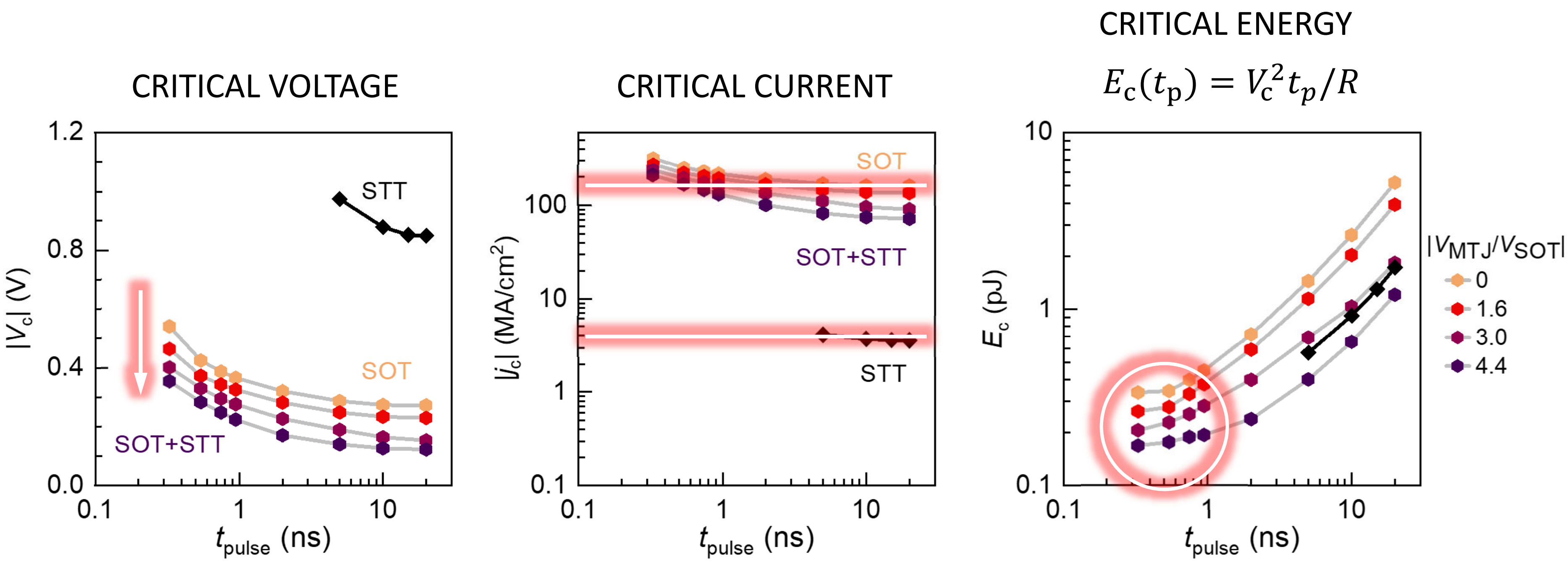

Writing by combined V_{SOT} & V_{MTJ} pulses provides gain in speed and energy efficiency

Krizakova et al., *Phys. Rev. Appl.* **15**, 054055 (2021)

Quantifying the separate effect of SOT, STT, VCMA, and SELF-HEATING

- Critical SOT voltage: $V_c(V_{\mathrm{MTJ}}, t_p)$

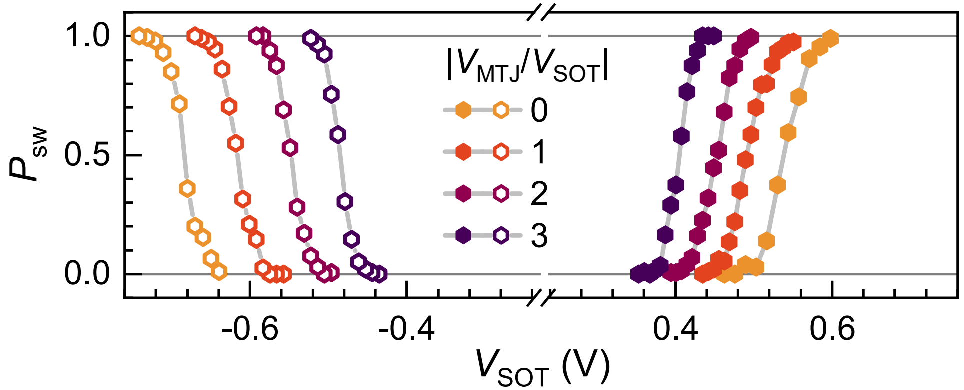

- Normalized critical voltage: $v_c = V_c/V_{c0} = (V_{c0} + \Delta V_c)/V_{c0}$

$$v_c = 1 - \left(\underbrace{\frac{2\,\varepsilon}{M_S t_{\mathrm{FL}}\, t_{\mathrm{MgO}}} V_{\mathrm{MTJ}}}_{\text{VCMA}} \pm \underbrace{\frac{\beta}{RA(1 - b|V_{\mathrm{MTJ}}|)} V_{\mathrm{MTJ}}}_{\text{STT}} + \underbrace{\frac{\zeta}{RA(1 - b|V_{\mathrm{MTJ}}|)} V_{\mathrm{MTJ}}^{\,2}}_{\text{Joule heating due to } V_{\mathrm{MTJ}}}\right) \cdot (H_{\mathrm{k}} \mp H_{\mathrm{offset}})^{-1}$$

Krizakova et al., *Phys. Rev. Appl.* **15**, 054055 (2021)

3-terminal MTJs: combining four effects in one device

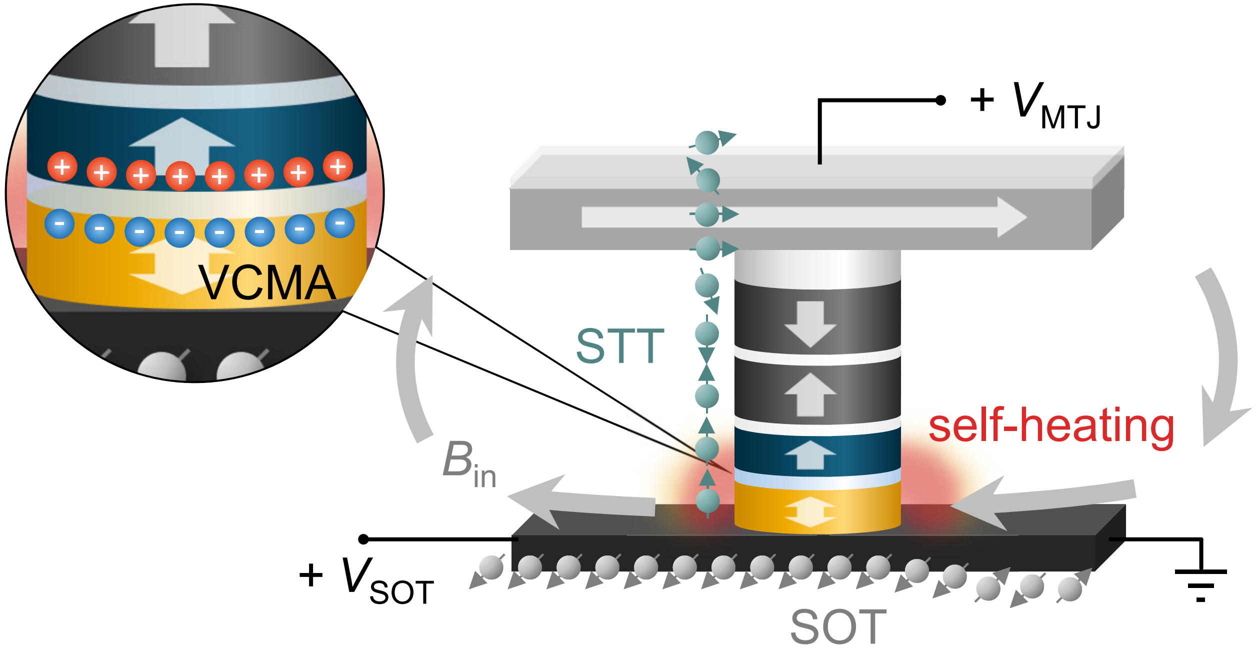

SOT	$\propto j_{SOT} \propto V_{SOT}$
STT	$\propto j_{STT} \propto V_{MTJ}\,\mathrm{sign}(M_{REF})$
Joule heating	$\propto I^2 R$
VCMA	$\propto V_{MTJ}$

Krizakova et al.,
Phys. Rev. Appl. **15**, 054055 (2021)

Dense integration of 3-terminal MTJs for SOT-MRAM: "VGSOT"

VCMA
SELECTOR

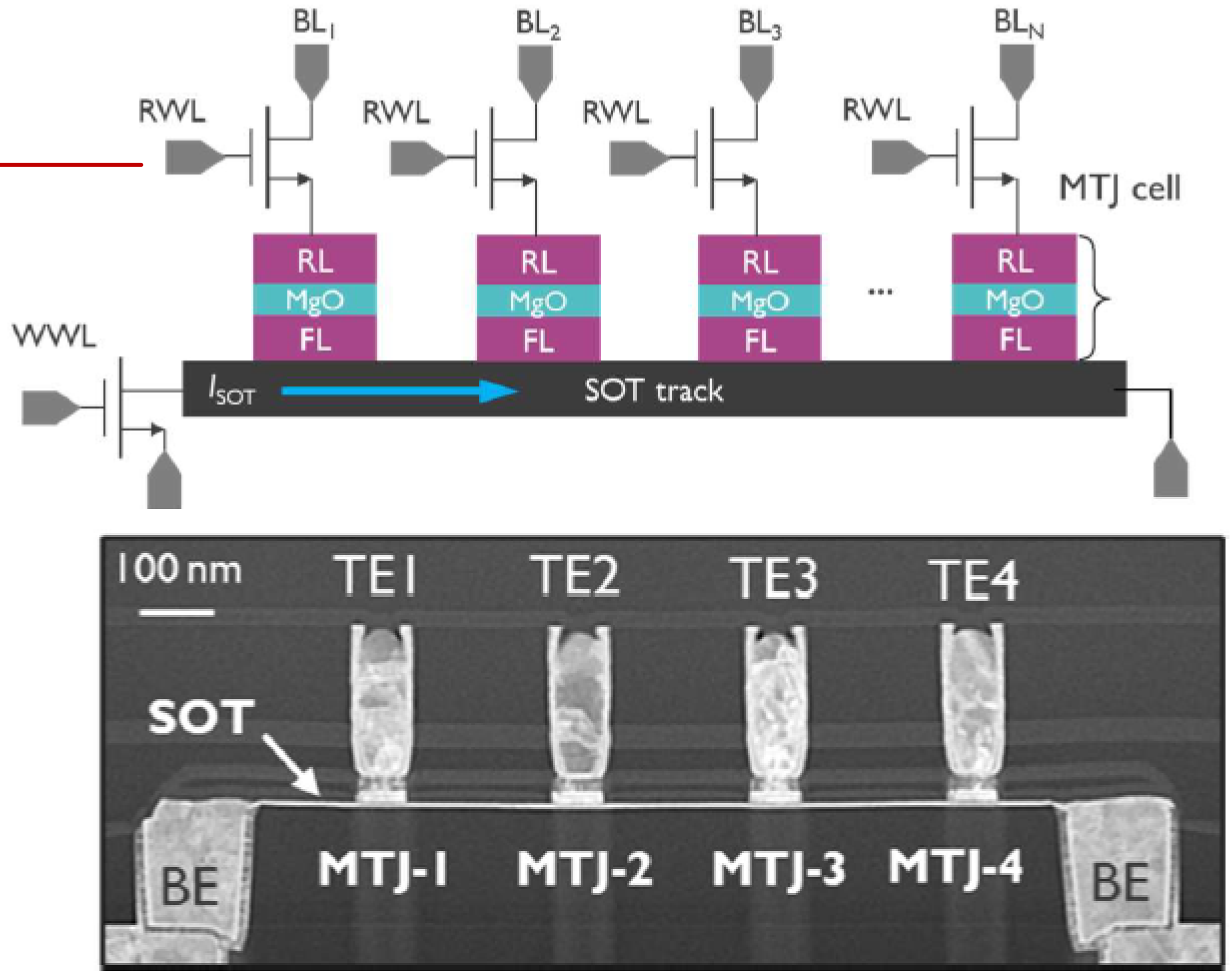

Cai et al., *VLSI Tech. Circ.* 375 (2022)

imec

Embedded memories: Future

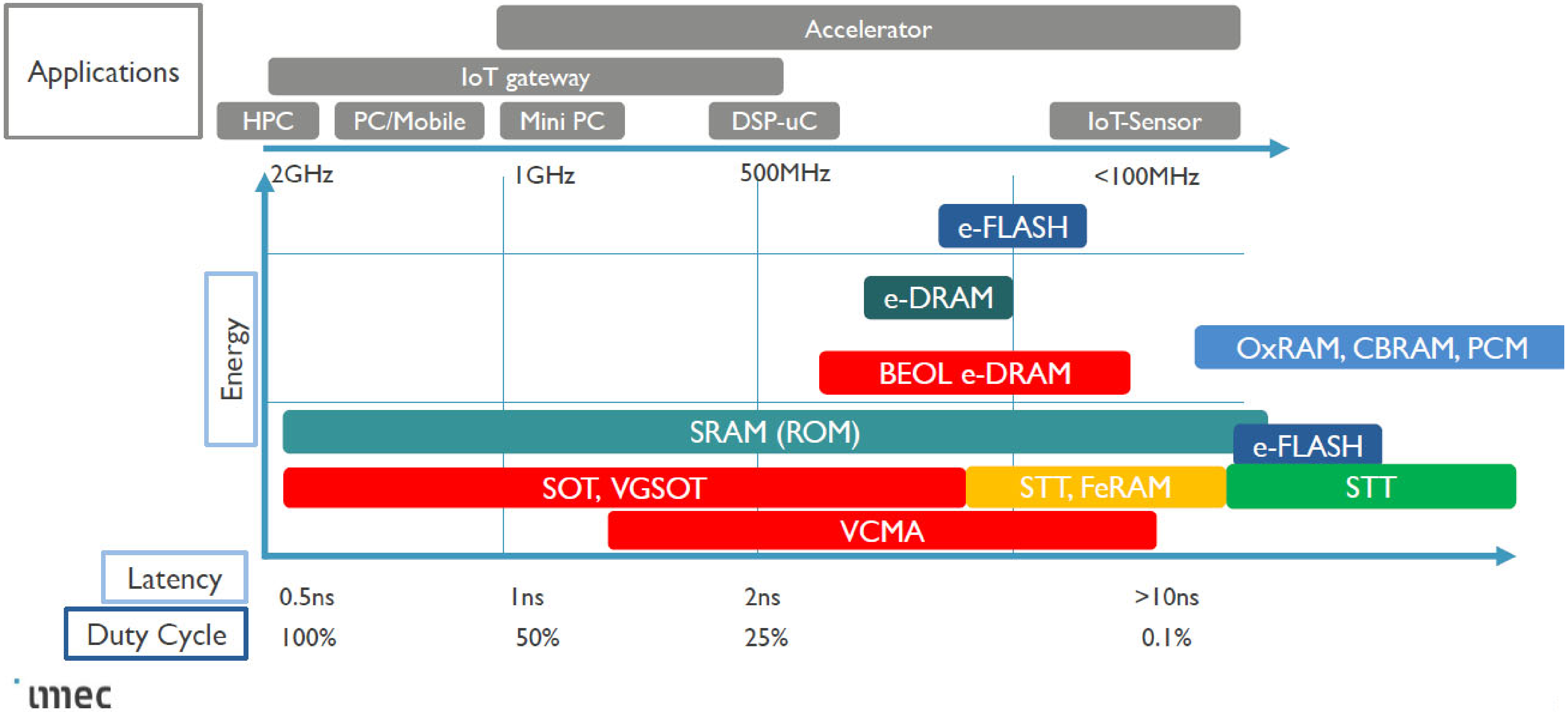

Conclusions

Current-induced spin and orbital moments

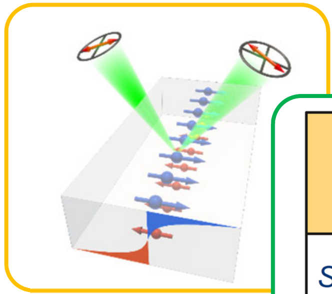

Orbital-to-spin conversion

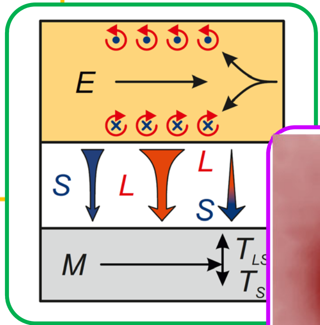

Current-driven DW and skyrmion motion

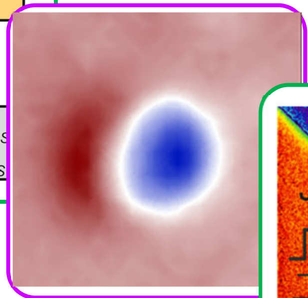

Current-driven dynamics in ferrimagnets

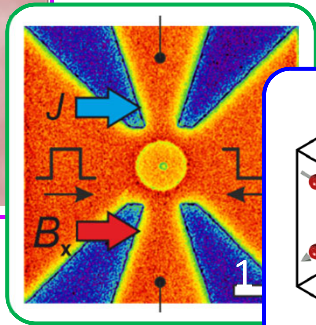

Chiral antiferromagnets

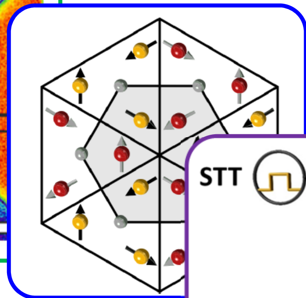

3-terminal MTJs

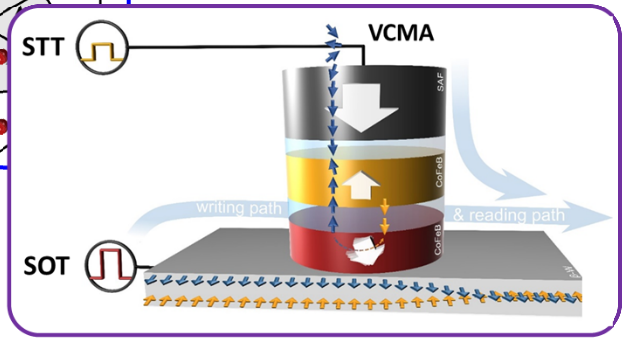

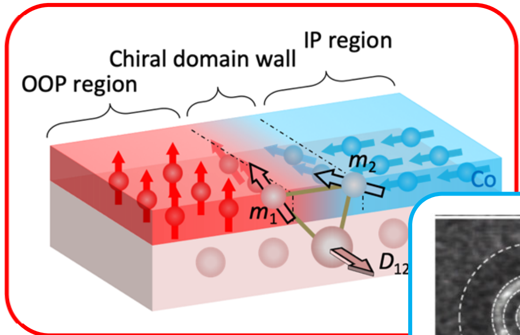

DMI-coupled nanomagnets

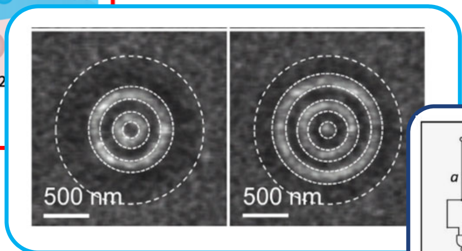

Synthetic magnets

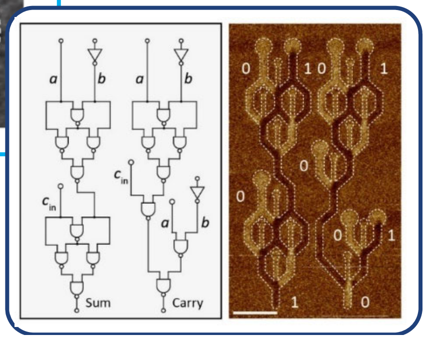

Electrically-driven
domain wall logic circuits

Material issues: SOT efficiency vs power density

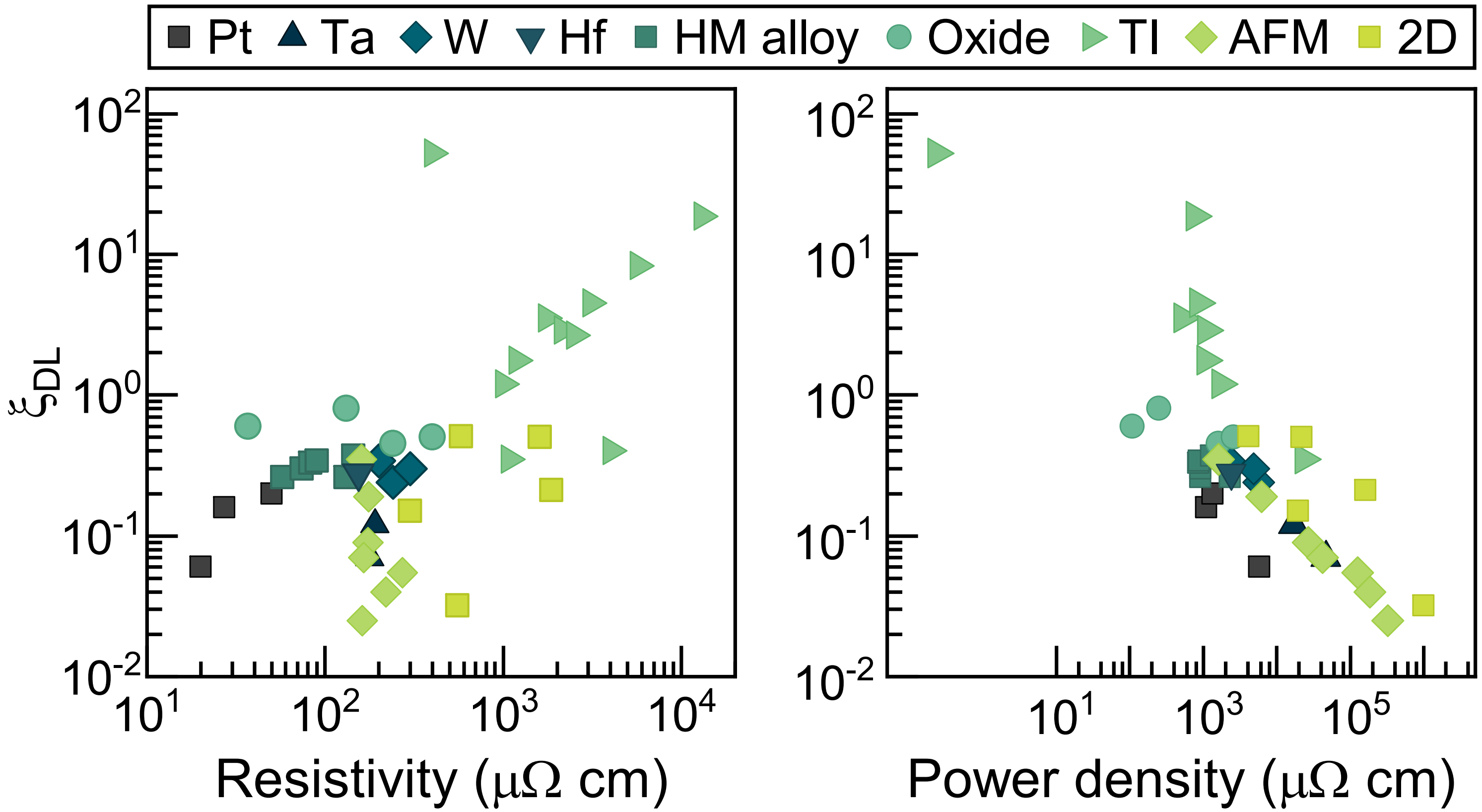

SOT efficiency ξ_{DL}

$P_{SW} = j_{SW}^2 \rho \propto \frac{\rho}{\xi_{DL}^2} \propto$ magnetic anisotropy

Krizakova, PG *et al.*, *J. Magn. Magn. Mater.* **562**, 169692 (2022)

Materials with large SOT efficiency

Switching power density:

$$P_{SW} = j_{SW}^2 \rho \propto \frac{\rho}{\xi_{DL}^2}$$

Spin-orbit torque efficiency:

$$\xi_{DL} = \frac{j_s^{FM}}{j_c} = \frac{2e}{\hbar} M_s t_{FM} \frac{B_{DL}}{j_c}$$

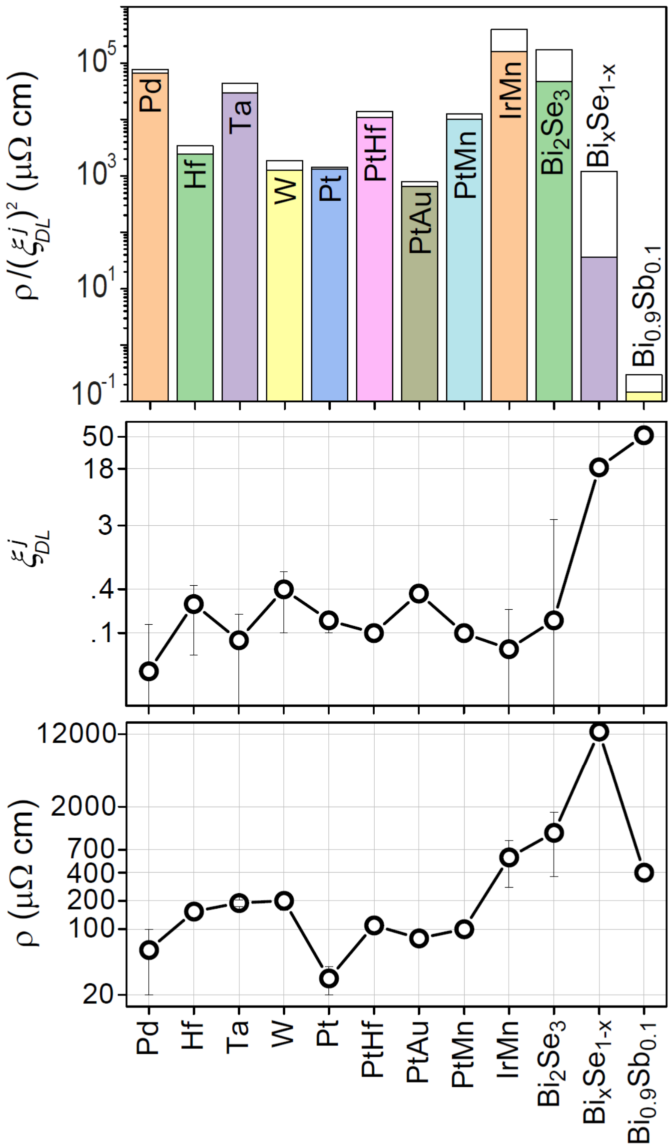

Bi_2Se_3/NiFe	IP	$j_{sw} = 0.6$ MA/cm^2	Wang et al., Nat. Comm. **8**, 1364 2017
$Bi_xSe_{(1-x)}$/CoFeB/Gd/CoFeB	OOP	$j_{sw} = 0.4$ MA/cm^2	Mahendra et al., Nat. Mater. **17**, 800 (2018)
$Bi_{0.9}Sb_{0.1}$/MnGa	OOP	$j_{sw} = 1.5$ MA/cm^2	Khang et al., Nat. Mater. **17**, 808 (2018)
$[Pt/Hf]_N$/Pt/Co	IP	$j_{sw} = 3.6$ MA/cm^2	Zhu et al., Phys. Rev. Appl. **11,** 061004 (2019)

Manchon et al., Rev. Mod. Phys. **91**, 035004 (2019)

Conversion efficiency in TIs: twin-free single crystal $Bi_{0.9}Sb_{0.1}$

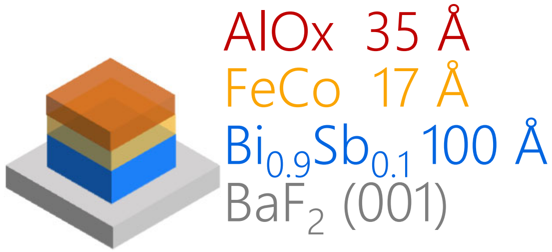

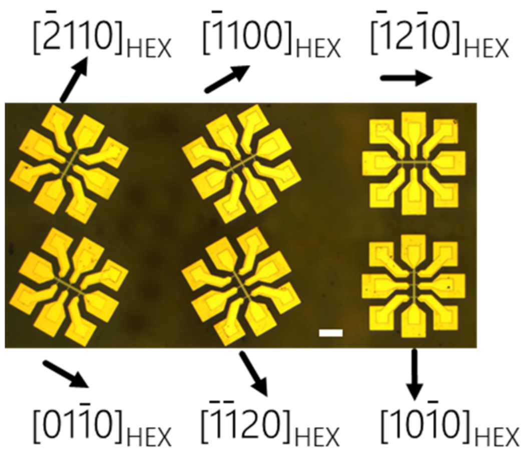

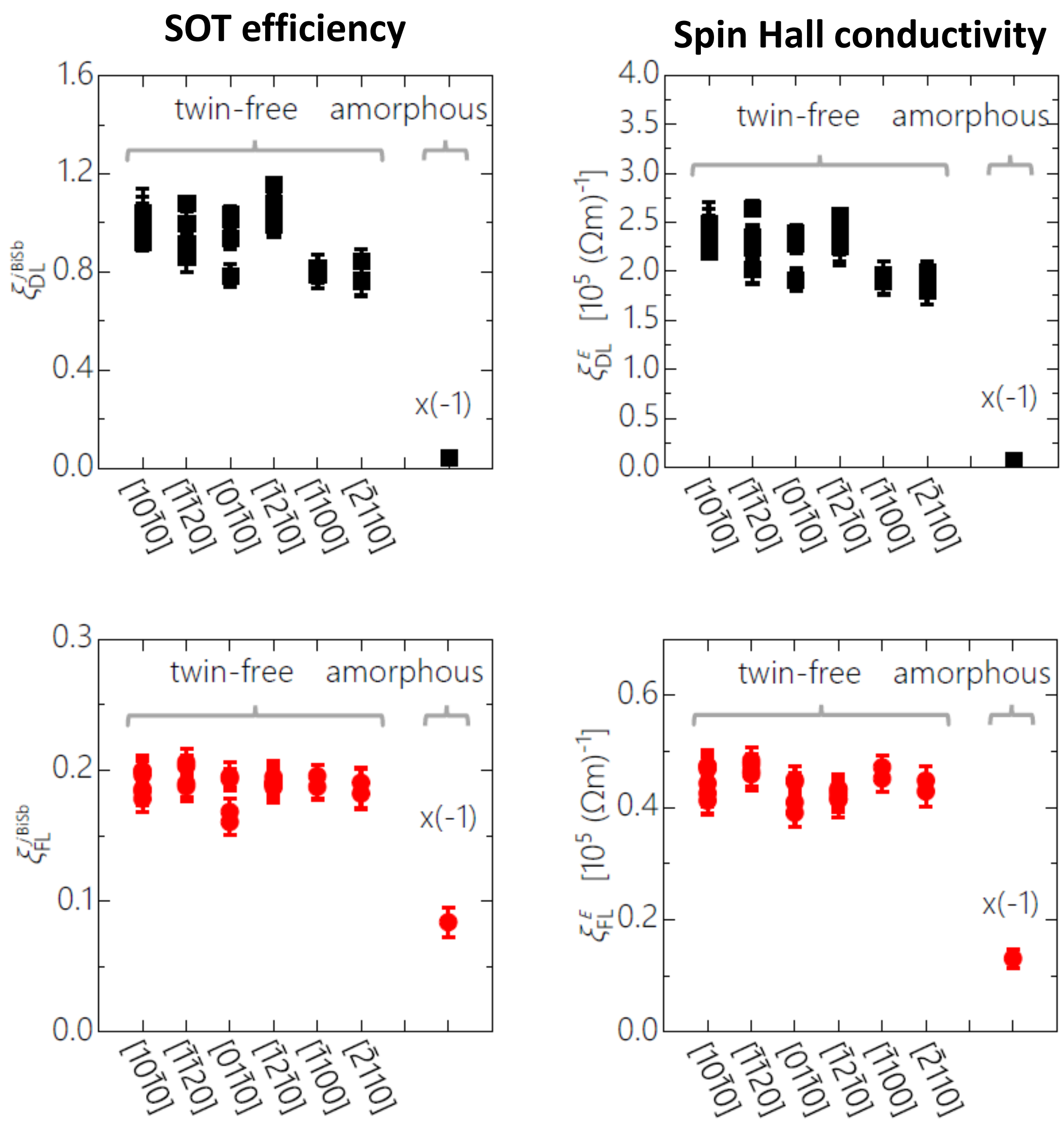

- $\xi_{DL} \approx 1$ (single crystal),
- $\xi_{DL} \approx 0.05$ (amorphous)
- Isotropic
- Nonmonotonic *T*-dependence

Binda et al., Adv. Materials 2023